Doctoral Thesis

Design of Highly Stable 1D/2D Nanostructure-Based Transparent Conducting Electrodes

Hyung Duk Yun

School of Material Science and Engineering

Graduate School of UNIST

2018

Design of Highly Stable 1D/2D Nanostructure-Based Transparent Conducting Electrodes

Hyung Duk Yun

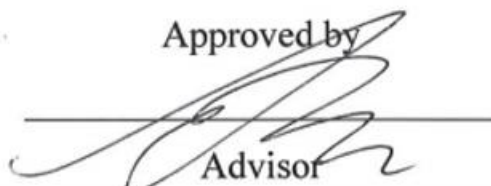**School of Material Science and Engineering**

Graduate School of UNIST

Design of Highly Stable 1D/2D Nanostructure-Based Transparent Conducting Electrodes

A thesis/dissertation

submitted to the Graduate School of UNIST

in partial fulfillment of the

requirements for the degree of

Doctor of Philosophy

Hyung Duk Yun

6. 14. 2018 of submission

Approved by

_____

Advisor

Soon-Yong Kwon

Design of Highly Stable 1D/2D Nanostructure-Based Transparent Conducting Electrodes

Hyung Duk Yun

signature

Advisor: Soon-Yong Kwon

signature

Lee Soon Park

signature

Kibog Park

signature

Heungjoo Shin

signature

Young-Min Kong

Abstract

In recent of days, indium tin oxide (ITO) has been extensively used for a transparent conducting electrodes (TCEs) in various opto-electronic applications; such as touch screen panels (TSP), transparent conducting electrodes (TCEs), flat panel displays etc. However, ITO have limitations in the emerging new technology point of view for flexible display applications. Despite its excellent opto-electronic property, expensive cost and weak mechanical property against bending hinder its application of next generation TCEs. Numerous suggestions were made for new TCE materials, including metal nanogrids, metal nanowires, conducting polymers, carbon nanotubes (CNTs), and graphene (Gr). Yet, alternative material properties do not match up with commercial demands for transparent conducting electrodes (TCE). For instance, metal nanowires comprised with silver, gold, and copper (Cu) have been reported and demonstrated for TCEs applications. However, the contact resistance between each nanowire, light scattering under visible wavelength, and instability under ambient condition hinder its opto-electronic property. Conducting polymer have been generally used for its high electrical properties and simple processing method; however, week endurance under humid and high temperature condition is always problematic for commercial application uses. graphene has been spot-lighted since year 2010 after noble prize was rewarded. The excellent opto-electronic, mechanical properties, and long-term stability were more than enough to grab many researcher's attention. Although, intense studies on Gr were performed, its opto-electronic properties were never better when compared with ITO due to various unavoidable defects. This thesis presents three research objectives. First, high quality single layer graphene (SLG) with single-walled carbon nanotube (SWCNT) TCE was fabricated and demonstrated for a wearable device application. By introducing effective coating method of SWCNTs on a SLG surface, defective sites were well filled and bridged with SWCNT enhancing the performance of the SWCNT/SLG composite film. Second, silver nanowires (AgNWs) were synthesized by using a modified polyol with continuous flow method for an industry scale production level. Unlike previous studies, AgNW reaction solutions were inserted through a milli-capillary tube for AgNWs reaction, and stable synthesis of AgNWs were observed for more than 8 hours. Finally, highly stable multi-layer graphene (MLG)/AgNW/polyimide (PI) composite film was fabricated to propose ITO alternative materials for future applications. The high crystalline MLG/PI provided excellent barrier properties to protect embedded AgNWs under various environments including high temperature, humid, and sulfurization conditions. By accomplishing these three objectives, this research has proposed the combination and usage of current new materials all together for practical implementation in the industry level.

Contents

List of Figures

(1 ml)/graphene/PET composite bent at (f) 1000 and (g) 2000 times.

located at the bottom of a quartz tube. Additionally, size of multilayer graphene flakes increased when a copper foil was oxidized. (d) Dependence of multilayer graphene coverage data by copper oxidation method. (e) Relationship between back side graphene coverage and copper foil oxidation method after graphene growth. (f) Relationship between multilayer graphene coverage data with growth time.

Figure 4-5. (a) Photo and schematic images of Al_2O_3 substrate wrapped by a copper foil. (b-c) Optical microscope images of graphene/copper foil after 200 ˚C annealing treatment. (d) An optical microscope image of graphene transferred on a Si/SiO$_2$ substrate.

Figure 4-6. (a) A schematic illustration of MLG/AgNW/PI fabrication method. (b) a photo image of the composite film held by tweezer. (c-d) SEM images of MLG/AgNW/PI composite film. A purple and green arrow indicate graphene tear and wrinkle. (f) Raman spectrum of MLG grown on a Cu foil

Figure 4-7. (a) An opto-electrical data of a Gr/PI composite film. Both transmission and sheet resistance value decreased as multilayer graphene portion on a single layer graphene increased. (b) An opto-electrical data of a multilayer graphene/AgNW/PI. When spin-coating number of AgNW increased, reduction of sheet resistance and transmittance were observed. (c) Effect of sheet resistance reduction after welding of AgNWs on a multilayer graphene/AgNW/PI composite. (d) Transmission and sheet resistance data comparison with other transparent conducting electrodes.

Figure 4-8. Mechanical properties of multilayer graphene/AgNW/PI composite film. (a) bending cycle, and (b) bending radius.

Figure 4-9. Environmental test of multilayer graphene/AgNW/PI at (a) 100 ˚C under ambient condition, (b) room temperature under ambient condition, and (c) sulfurization by immersing the composite film in ammonium persulfate solution

Chapter 1. INTRODUCTION

1.1 The Importance and Current Status of Transparent Conducting Electrodes

Transparent conducting electrodes (TCEs) are thin films comprised of optically transparent and electrically conductive materials. It is one of the most important components in opto-electronic devices including solar cells, light emitting diodes, liquid crystal displays, touch screens, and organic light emitting diodes. With the ever-increasing demands of these devices, the overall TCE market will tremendously grow. The traditional and mostly used material for TCEs are doped metal oxides. Among them, indium tin oxide (ITO) has been market leader in the field for decades due to its excellent transparency and electrical property[1]. However; despite its high performance as thin films, the use of ITO and relying on this material for the fabrication of low-cost devices has many drawbacks[2]. Cost is a primary issue in both raw material cost and in deposition methods. For instance, indium is a rare metal which the resource is limited and the price of indium metal in dollars are continuously arising. The sputtering process by which ITO is deposited onto a substrate is also expensive and time-consuming. Commercially-produced ITO is deposited by DC sputtering method under vacuum system rather than cheap coating method such as solution process. Various optoelectronic devices including photovoltaics, organic-light emitting diodes are now requiring flexible, lightweight devices built on a transparent polymer substrate. ITO can be sputtered in a roll-to-roll structure; however, the performance of ITO is limited on the polymer substrates due to the heating requirement for the low sheet resistance. In addition, ITO is inherently brittle and weak under bending[3]. Such bending can result in microscopic cracks which may begin to form and propagate on the surface increasing its sheet resistance. This is a significant disadvantage for applications in which the final device structure is supposed to be flexible, bendable, or foldable, especially when many industries now days have significant interest on wearable devices. For next generation TCEs applications, researchers are prompted to look elsewhere for alternative TCEs materials development which are cheap and perform better with long-term stability and can be deposited on flexible substrates.

1.2 Flexible Alternatives to Indium Tin Oxide

There are various alternative materials studied for replacement of ITO, and they include metal nanowires[4], conducting polymers[5], carbon nanotubes (CNTs)[6], and their composites. Silver nanowire (AgNW)[7] synthesized with high aspect ratio shows very high electrical and optical conductivity, and only requires simple fabrication process with environment-friendly solution-based synthesis method. They are also easy to scale up for various industry applications. Typically, the opto-electrical property of AgNW-based TCEs can be enhanced by decreasing the diameter and increasing the length of AgNWs since narrow nanowires scatter less light and increasing aspect ratio decrease the number of high-resistance nanowire-nanowire contacts in the film. Yet, there are numerous limitations which must be overcome before its practical applications. Solution reaction based AgNW synthesis method often leave polymer residues on AgNW side walls which increases contact resistance during the film formation. The contact resistance of each nanowire is significantly problematic, thus post welding treatment is necessary for practical applications. They also show weakness at oxidation and sulfurization under ambient conditions. Conducting polymers are also one of the alternatives that can replace ITO and its application for TCEs were studied widely. Synthesis of poly3,4-ethylenedioxythiophene (PEDOT) by using vapor phase polymerization (VPP)[8], electro-polymerization (EP)[9], and oxidative chemical polymerization methods[10] has been reported and their conductivity often varies around 3300 $S \cdot cm^{-1}$. Their electrical properties can be further enhanced by various methods such as; secondary doping[11] by treating with nitric acid or sulfuric acid, or ultraviolet irradiation (UV)[12] treatment. However, long-term environmental stability often lacks and show degradation under high temperature, humid condition. Graphene has received huge interests in various research fields for unique properties. They include high carrier mobility, low electron-phonon scattering, quantum Hall effect, and ambipolar electrical field effect. They are also known to possess excellent mechanical durability which is thought to present better performance than any other 2-dimensional material and high transparency of single layer graphene (SLG) only shows 2.3 % absorption of visible light. Recently, it was reported by many scientists that graphene can be introduced in various applications such as energy storage materials, field effect transistors, cell imaging, barrier materials, chemical and bio-sensors, TCEs, and more. Although the theoretical calculation and analysis of graphene propose that it would perform as an excellent TCEs, chemical vapor deposition (CVD) grown high crystalline and large area graphene often present a higher sheet resistance value, than ITO-based TCEs. This was attributed to the structural defects such as tears, grain boundaries, wrinkles, folds, and point defects in the CVD grown as-processed graphene layers **(Figure 1-1a-f)**. Such defects can hinder the delocalization of electrons in sp^2 orbital and lead to trapping or charge scattering. Although various methods such as large graphene domain growth by optimizing the growth conditions or controlling the stitching of graphene domains by engineering the orientation of the underlying copper surface have been tried to minimize the negative effects of various

defective sites in the graphene grown by using a CVD method, its reduced property hinder various TCEs practical applications. In other approaches, combining graphene with other conducting materials, such as conducting polymers, metal nanowires, and metal grids can enhance the performance in the CVD grown graphene while preserving its high transparency.
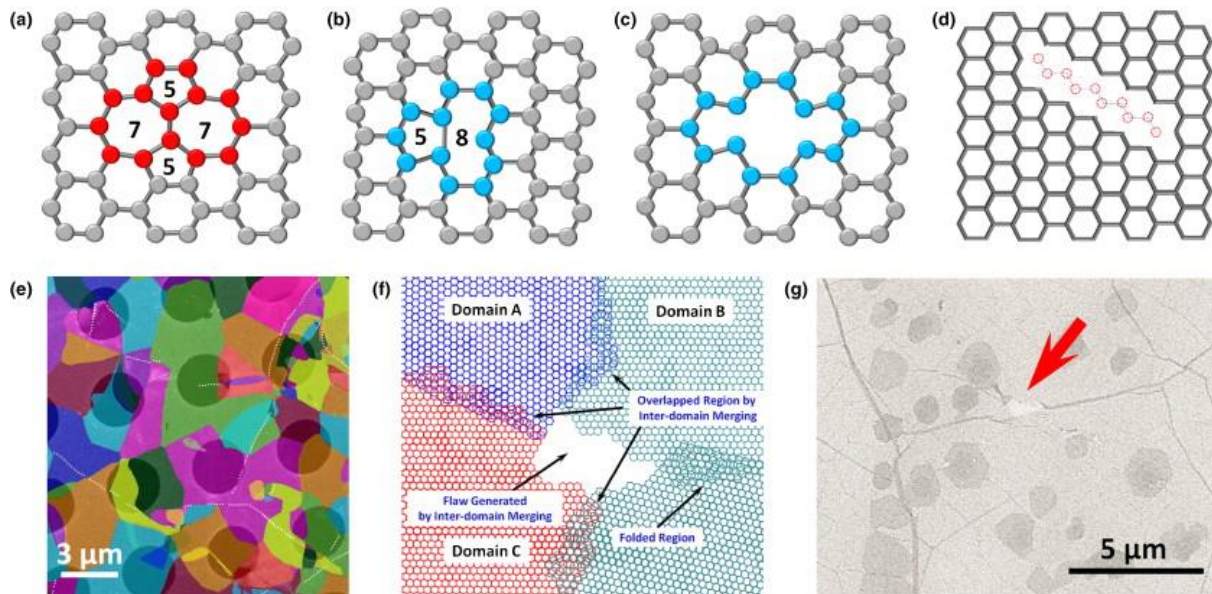
Figure 1-1. Defects in graphene. (a) Stone-Wale defect, SW (5577). (b) Mono-vacancy. (c) Di-vacancy. (d) Line defect formed by aligned vacancy structures. (e) Grain boundary mapping of polycrystalline CVD graphene. (f) Flaw generated by partial surface coverage of the CVD graphene. (g) Macroscopic defect created during the transfer process.[13]

1.3 Research Goals

Excellent properties with various materials are being proposed in now day; however, they suffer from long-term stability, and trade-off characteristic between electrical property and transmittance. Since conducting polymers and metals are easily degraded under high temperature and humid condition, and carbon materials lack in opto-electrical properties, hybrids of such materials may resolve critical limitations for TCEs applications. Among various techniques, combination of one-dimension materials with high crystalline graphene may overcome such problems by combining the merits of 1 dimension and 2-dimension transparent conducting materials. For instance, highly conducting CNTs can be incorporated with a high crystalline graphene for flexible electronics with electrical performance that presents better than organic semiconductors or amorphous silicon, due to the excellent intrinsic electrical properties of CNTs within the network. Introducing high crystalline graphene layers as a barrier film on metal nanowire based TCE could also be a solution. Although metal nanowire's opto-

electronic properties are comparable to ITO, their long-term environmental stabilities under ambient and harsh condition hinder its actual usage on various applications. High crystalline graphene is well known for excellent barrier film due to its chemical inertness and complete impermeability to water and oxygen. They are often used with metal electrodes to prevent from oxidation, corrosion, and degradation in electrochemical systems. The objectives of this thesis are (1) to propose simple and uniform coating method of single-walled carbon nanotubes (SWCNT) on a graphene/copper foil to fabricate SWCNT/graphene composite film for TCE applications, (2) to develop efficient, uniform and stable synthesis methods for AgNWs by using a continuous flow method in a tubular reactor, and (3) to propose potentialities of hybrid structure of multi-layer graphene/AgNW/polyimide (MLG/AgNW/PI) composite film for alternatives to ITO.

Chapter 2. Highly Stable Single-walled Carbon Nanotube/Graphene Composite Transparent Electrodes Containing Uniform Carbon Nanotube Networks

2.1 Introduction

The distinctive properties of graphene such as low electron-phonon scattering[14], high carrier mobility[15], ambipolar electrical field effect[16], quantum Hall effect[17], and excellent mechanical property with high transmittance under visible ranges[18], grabbed huge attentions in various research fields. Among many graphene growth methods, chemical vapor deposition (CVD) method is mostly used to obtain high crystalline and large are graphene layers. Yet, CVD grown graphene suffer from various defects during and after growth of graphene. Grain boundaries, wrinkles, tears, folds, and point defects are inevitable[19] with current technology and often present higher sheet resistance when compared to indium tin oxide (ITO) based transparent conducting electrodes (TCEs). Various efforts were shown to overcome such deleterious effect of graphene defect and incorporating conducting 1-dimensional nanomaterials can be one solution. Due to effective surface area and various coating methods, introducing conducting 1-dimension nanomaterials on a graphene may significantly enhance performance by providing conducting channel on the defective sites of graphene. Carbon nanotubes (CNTs) are one of the most studied materials in the past decades. The structure of CNTs are comprised of single or multi-layer graphene sheets wrapped into 1-dimension cylinder. CNTs are also famous for its amazing properties. For example, CNT possess high electron mobility (100,000 cm^2/Vs), high electrical conductivity (10^4 S/cm), high thermal conductivity (3500 W/mK), and excellent mechanical strength (individual mutli-walled CNT possess tensile strength of 100 GPa). These CNT networks performance generally depend on how they are arrayed. Thus, combining graphene and CNTs together may benefit each other and show excellent performance of TCEs. In this chapter, coating of uniform single-walled carbon nanotubes (SWCNTs) on a graphene will be discussed and elucidate enhanced graphene properties.

2.2 Coating and Growth Mechanisms

2.2.1 Coating Methods for Carbon Nanotubes

Although CNTs possess excellent properties, problems such as insulating residues, large aggregation, and non-uniformity upon coating may cause significant degradation on their performance when formed as networks of film. When CNTs are dispersed in a solvent, the high aspect ratio and strong interaction between each CNTs due to the van der Waals cohesive forces can result in aggregation and bundling[20]. Since many solutions based CNTs coating application require well-dispersed CNTs, such aggregation is a major drawback to make full use of their remarkable properties. The aggregation problems are often overcome by post-treatment on CNTs. For instance, incorporation of ionic surfactant[21], covalent attachment of hydrophilic groups[22], physical adsorption of amphiphilic molecules[23] is used widely. Uniform coating of CNT solution on a substrate is another challenging task. Various methods are well studied and reported. For example, spin coating involves the addition of the CNT solution on a target surface of substrate during a spinning[24]. Dip coating is facile and effective to coat CNTs on a planar substrate[25]. For better interaction and adhesion between CNTs and a substrate, CNTs and substrates are often functionalized for covalent bonding together[26]. Spray coating is one of the most used coating method for efficient and uniform coating of nanotube networks on a target substrate[27], where nanotubes are well dispersed in surfactants with organic solvents and sprayed-onto a heated substrate. Vacuum filtration[28] is widely used for forming a homogeneous network on its planar surface by forcing dispersion of CNTs on a planar surface of filter paper. Other techniques for CNT coatings include bar assisted coating[29], ink-jet printing[30], layer-by-layer (LBL) coating[31], and drop casting method[32]. In all methods, the surface property of a target substrate and the CNT dispersion play critical roles in the uniformity of the CNT network.

2.2.2 Chemical Vapor Deposition Growth of Graphene

Top-down, and bottom-up methods are well reported for synthesis of graphene layers. The CVD growth of high crystalline and large-area of single-layer graphene on metal films has been reported widely. Despite the significant enhancement in growth technology, graphene obtained by CVD method often possess poly-crystalline with various defects. For various applications, high crystalline and uniform graphene synthesis is inevitable. Until now, graphene films grown on transition metal substrate with high carbon solubility (cobalt[33], nickel[34], iron[35], platinum[36]) do not yield uniform monolayer graphene. In contrast, transition metal with low carbon solubility such as copper[37] is an excellent candidate for growth of uniform and large-area single-layer graphene films. Since graphene synthesis are generally based on catalytic and chemical reaction, the overall process of graphene is formed on the

surface of transition metal catalyst through adsorption, decomposition, and diffusion of carbon atoms. The high carbon solubility of transition metal can induce bulk diffusion of carbon, resulting in in-uniform multi-layer of graphene. However, surface-mediated growth of graphene is often observed when transition metal catalyst with low carbon solubility is used. In typical CVD graphene growth, various defects are introduced during and after growth of graphene. For example, copper foil used for graphene growth often possess impurities, copper steps, and facets, which are possible active sites for carbon adsorption and result in multilayer flakes[38] (The ad-layer of multilayer flakes have randomly oriented and may act as a scattering sites). The differences in thermal expansion coefficient and lattice constant of copper and graphene generate ripples and wrinkles on a graphene surface. In addition, the general wet transfer method by using sacrificial polymer layer may generate tears, folds, and artificial wrinkles.[40] Until now, these defects are impossible to prevent during/after the CVD graphene growth process; however, surface flattening treatment of copper or hydrophilic treatment of the target substrate may resolve such problems. Growth of large area single crystalline graphene layer is another excellent alternative solution to obtain defect free graphene layers. The growth of high crystalline and large area graphene is necessary for the next-generation optoelectronic devices, because the grain boundaries in poly-crystalline graphene can significantly disrupt the carrier transport performance due to the scattering effect[41]. In recent of days, there are several reports to grow grain boundary free graphene. For example, large size single crystalline graphene can be grown by either suppressing the nucleation density[42] or induce the graphene growth orientation alignment with perfect stitching of graphene domains[43]. Such results are obtained by fine tuning of graphene growth conditions. For example, substrate roughness flattening, temperature control, chamber pressure control, reacting gas ratios, and oxygen pre-treatment prior to graphene growth. Although growth of high crystalline large area graphene showed striking result, it is necessary to develop effective growth process to apply CVD graphene for industrial applications.

2.2.3 Hybridization of Graphene and Carbon Nanotube

  Due to the hydrophobic surface of CVD grown pristine graphene layer, solution coating of CNTs often result in in-uniform coating; the composite film fabrication methods typically show large aggregation of coffee ring shape. For instance, CVD growth of CNTs and graphene can control structure and property effectively; however, high temperature process (~1,000 °C) is not compatible with polymeric substrates. Solution based coating of CNTs onto target substrates is an efficient and effective method for various flexible and wearable applications; however, fabrication of CNT/graphene composites by a such method is mostly fabricated by using graphene oxide (GO) or reduced GO materials. Spin and dip coating methods are facile and fast, but their uniformity is largely affected by surface hydrophilicity

which may cause aggregation of CNTs. Several reports for graphene carbon nanotube hybrid films have been demonstrated. For instance, Tung et al. reported incorporation of reduced graphene oxide (rGO) with carbon nanotube for high-performance transparent conductor[44]. One step growth of graphene and carbon nanotube in CVD was demonstrated by Dong et al. [45], and Yu et al[46]. illustrated self-assembly of multi-walled carbon nanotube (MWCNT) with reduced graphene oxide (rGO) nanosheets. Kim et al. established hybrid film of graphene carbon nanotube by spin coating carbon nanotube on a copper foil and synthesized graphene to obtain hybrid film and enhanced electrical properties[47]. However, previous approaches are mostly limited for graphene oxide and reduced graphene oxide where functional groups are necessary and exhibit high sheet resistance due to the presence of defects. Recent reports of fabricating CVD grown graphene and carbon nanotubes composite film suggest that the it is necessary to comprehend and design CNT networks arrangement to control the performance of carbon-based TCEs and further improvements in sheet resistance, transmittance for commercial flexible TCEs applications.

2.3 Experiment

2.3.1 High Crystalline Graphene Growth

High crystalline large area single layer graphene was grown by using a conventional CVD process method. In brief, electropolishing technique was applied on a copper foil with 25-μm thickness (Alfa Aesar, 99.8 % purity) for 15 min for smooth surface. Then electropolished copper was rinsed with distilled water and isopropyl alcohol. The pre-treated copper foil was loaded into a quartz tube for CVD graphene grown and the chamber was pumped to low vacuum. Before graphene growth on a copper foil, the temperature was increased to 1,050 °C within 35 min while H_2 gas flowing (270 mTorr) and maintained for 15 min to remove various forms of oxides in copper foil. The single layer graphene was grown by flowing CH_4 and H_2 gas (1:2 ratio, 86 mTorr) for 10 min. After single layer graphene growth by using CVD method, graphene was transferred to a transparent PET substrate by using sacrificial layer of poly(methyl methacrylate) (PMMA) coating on a graphene/copper assembly and a copper foil was completely etched in an etchant solution of 0.1 M $(NH_4)_2S_2O_8$. After etching of copper foil is completed, the remaining PMMA/graphene film was rinsed with distilled water and transferred onto a PET substrate. The remaining water in between PMMA/graphene and PET was completely dried on a hot plate at ~100 ˚C for 10 min. Finally, the sacrificial layer of PMMA was dipping the composite into acetone solvent for 10 min. For better transfer of CVD grown graphene on a PET substrate, oxygen plasma treatment was applied on a PET which made it became more hydrophilic and this process enhanced wetting characteristic which helped water to efficiently evaporate in between graphene and PET substrate during wet-transfer process. The oxygen plasma treatment on a PET substrate helped to

obtain well transferred graphene/PET composite by using wet-transfer method, with less generation of various defects in graphene such as folds, wrinkles, tears and ripples.

2.3.2 Spray Coating of Single-walled Carbon Nanotubes and Fabrication of Single-walled Carbon Nanotube/Graphene Composite

In this work, spray coating was applied for uniform coating of CNTs on a graphene surface. By optimizing temperature of a target substrate during spray-coating process, large aggregation and coffee-ring effect were prevented and uniform coating of CNTs were obtained. As shown in the Figure 2-1, spray coating of SWCNTs were proceeded to achieve uniform coating of SWCNT networks on a graphene surface. First graphene was grown on a copper foil by using a CVD method. The obtained graphene/copper composite was then put on a hot plate for SWCNT deposition. For SWCNT coating, well dispersed SWCNT solution (SWCNT content: 0.3 wt. %, average length: 20 μm, average diameter: ~1.4 nm, sodium dodecyl sulfonate (SDS)-based water mixture) was spray coated on a graphene/copper substrate with varying solution amount from 1 to 4 ml by using an air compressor. The distance of air-sprayer nozzle to target substrate was set at ~11.5 cm and constant compressed air was supplied from an air compressor during the coating process. To remove insulating surfactant, the SWCNT coated graphene/copper composite was washed with highly purified water for 30 min. After etching copper by floating the composite on an ammonium persulfate solution, SWCNT/graphene composite was transferred onto a transparent PET substrate. To remove surfactant which was deposited during coating of SWCNTs solution, the SWCNT/graphene/PET composite was treated with diluted nitric acid (12 M) for an hour. Finally, the SWCNT/graphene/PET composite was washed with highly purified water for 30 min to prevent any chemical/molecular doping from nitric acid.
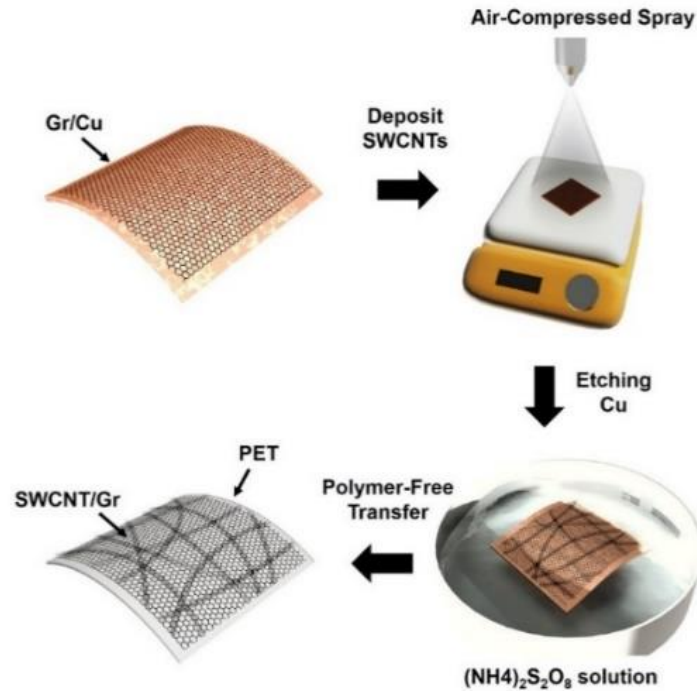
Figure 2-1. Schematic illustration of SWCNT/graphene composite film fabrication by air-spray coating of SWCNT solution on a single layer graphene grown by using a CVD method. The SWCNT/graphene/copper composite was first etched with copper etchant and transferred to a PET substrate treated with oxygen plasma.

2.3.3 Gold Chloride Doping of graphene and Single-walled Carbon Nanotube/Graphene Composite

Chemical doping of $AuCl_3$ was performed by dissolving $AuCl_3$ in nitromethane solvent at 20 mM concentration and spin-coating was performed on a graphene or SWCNT/graphene composite at 3,000 rpm for 30 seconds with a residual time of 30 seconds.

2.4 Figure of Merits

2.4.1 Surface Characterization and Crystalline Analysis of a Single Walled Carbon Nanotubes and a Graphene Layer by Using a Scanning electron Microscope and Raman Spectroscopy

We observed the uniformity difference of SWNCT networks was highly dependent to either deposition method or post-treatment methods (Figure 2-2). As it can be seen from the Figure 2-2, the highly uniform SWCNT networks on a graphene was formed by appropriate heat treatment during the coating process. It was noted that when SWCNT solution was evaporated at short period of time after spray coating, highly uniform SWCNT networks on a graphene was observed. When SWCNT was air spray

deposited on a graphene, we observed fine droplets of SWCNT solution accumulating due to low evaporation speed of solution. The accumulated SWCNT solution left an aggregated shape, which is often observed from the pattern of the capillary flow. It was clearly observed that SWCNT solution pinned at the edges of the droplets while slow drying, and this resulted in solid contents of the solution piled to the edge while solution evaporate from the edges. This resulted in the high density of SWCNT stains were left as a ring shape structure. Thus, it is very important to control the solution evaporation speed to obtain highly homogenous SWCNT coating on a graphene layer. We attempted to control the solution evaporation speed by changing the heating temperature of the graphene/copper during the air spray deposition of SWCNT solution. When heating temperature was below 100 ˚C, the as-synthesized films showed large aggregates of SWCNTs with coffee ring effect as indicated by SEM images. In contrast, when SWCNT solution was coated on a graphene/copper composite at 120 ˚C, uniform SWCNT networks were obtained.
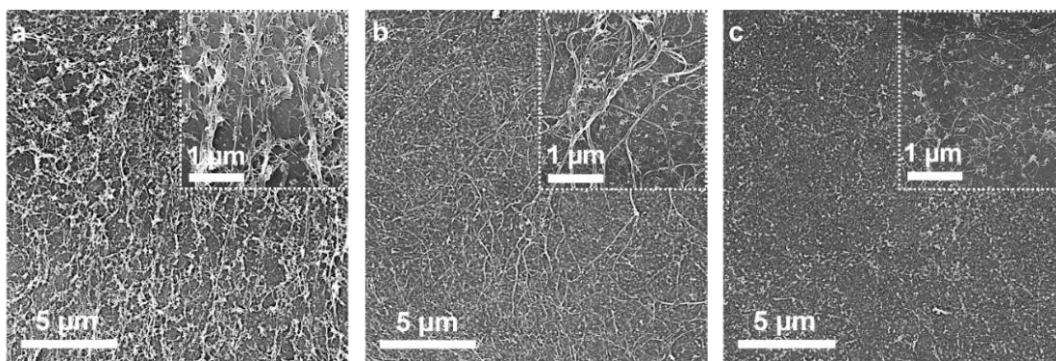
Figure 2-2. Morphology change observation of air-spray coated SWCNT networks on a graphene/PET composite with varying temperature of a hot-plate. During air-spray coating of SWCNT solution, the composite was heated, and the temperature was varied at (a) 40 ˚C, (b) 80 ˚C, (c) and 120 ˚C respectively.

The various defects on a single layer graphene were observed by SEM as shown in Figure 2-3a. During the growth of graphene, thermal expansion coefficient difference between graphene and copper substrate induced wrinkles which was indicated by a black arrow. Tears and folds were generated during graphene wet-transfer process which was indicated by a red arrow. These defects are main reason of graphene property degradation by scattering electrons. Figure 2-3b show study of graphene crystallinity by using a Raman spectroscopy. In Raman spectroscopy analysis, clear peaks of D,G, and 2D bands of graphene can be obtained and quality can be interpreted. Since this experiment was aimed for TCEs application, graphene was transferred on a transparent polymer substrate (PET). Since, Raman signals of typical graphene signals appeared with Raman signals of the PET substrate, graphene was transferred onto a Si/SiO$_2$ substrate to obtain clear Raman signals of graphene. The CVD grown graphene

transferred on a Si/SiO$_2$ substrate only showed the Raman D band (~1365 cm^{-1}) of graphene at line defects, which implies graphene with high crystallinity was grown by using our CVD process method. The intensity ratio of the G and 2D bands centered (~1575 cm^{-1} and ~2680 cm^{-1}, respectively) (I$_G$/I$_{2D}$ ~0.5) and the full width at half maximum (FWHM) of the 2D band (~28 cm^{-1}) indicate single layer graphene with high crystallinity was obtained.
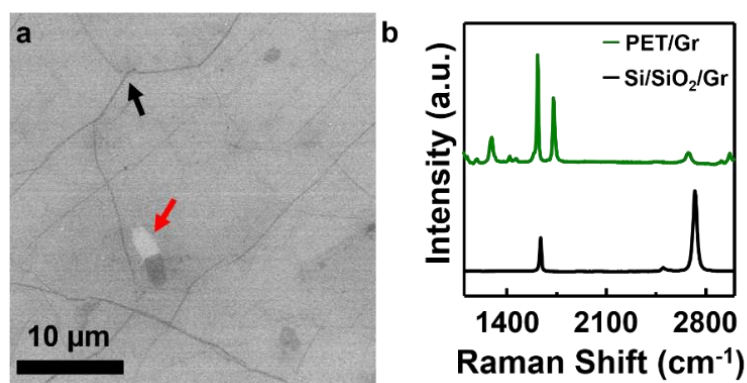
Figure 2-3. (a) A Surface image of single layer graphene/PET composite observed by using a SEM. (b) Raman spectra of a CVD grown single layer graphene from a copper foil and transferred on a PET and Si/SiO$_2$ substrate.

2.4.2 Opto-electronic Property of a Single-walled Carbon Nanotube/Graphene Composite

With effective and simple spray coating method, highly uniform SWCNT networks were formed on a graphene/PET composite. It can be also noted that density of SWCNT networks were controlled easily by changing the volume of SWCNT coating solution (Figure 2-4a,b). A SEM image of Figure 2-4c indicates the surface image of air-spray deposited SWCNT on a graphene layer which effectively filled the various defects on a graphene such as voids/tears (indicated by red dotted line) or folds (indicated by blue dotted line) and effectively bridged line defects (indicated by white arrow) in as-processed graphene. This effective coating of SWCNT minimized the deleterious effect from various defects in the CVD grown single layer graphene. It is also noted that SWCNT/graphene composite without any polymer coating retained its shape and structure on a copper etchant solution after etching copper foil in an ammonium persulfate etchant (Figure 2-4d). In general, CVD grown graphene requires sacrificial polymer coating due to its weak mechanical properties; however, our method enables the polymer-free transfer of the SWCNT/graphene composite onto the target substrates. This technique provides SWCNT/graphene composite film with less polymer residues than the conventional transfer method of sacrificial polymer coated graphene film, which could be potentially applied for 2-dimensional and carbon based next generation flexible electronics, sensors and display devices. When spin-coating was applied for SWCNT coating on a graphene film, the composite without sacrificial polymer coating was

broken apart during copper etching process. This was attributed to an inhomogeneous coating of SWCNTs, as shown in the inset of Figure 2-4d. The electrical and optical properties of the SWCNT/graphene/PET composite were evaluated by changing the SWCNT solution quantity. By varying the quantity of SWCNT solution with 1 ml steps, it was observed that SWCNT density on the graphene layer was effectively controlled by using air spray deposition method which resulted in the equidistant intervals of transmittance of the SWCNT/graphene/PET TCEs at 550 nm, as shown in Figure 2-4e. By controlling the SWCNT density on a graphene layer, a trade-off between the optical and electrical properties was observed. Since pristine single layer graphene only absorbs approximately 2.3 % of visible light, the transmittance of the SWCNT coated graphene layer decreased from 97.3 ± 0.2 to 95.7 ± 0.5, 94.3 ± 0.7, 92.5 ± 0.8, and 90.8 ± 1.2 % at 550 nm and sheet resistance reduced from 775 ± 100 to 390 ± 35, 286 ± 30, 219 ± 25, and 215 ± 15 ohm/sq, as shown in Figure 2-4f. The saturation trend of sheet resistance value was observed when SWCNT solution with more than 3 ml was spray coated and this was due to SWCNTs pile up on SWCNT networks since there are less room to fit on the graphene layer as density of SWCNTs increases. For comparison, sheet resistance of as-prepared single layer graphene was measured (775 ± 100 ohm/sq) and SWCNT/PET composite fabricated by increasing the SWCNT solution by 1 ml steps showed $9,000 \pm 575$ to $1,769 \pm 200$, $1,200 \pm 125$, 552 ± 35 ohm/sq. We noted that the as-prepared air spray-coated SWCNTs on a single layer graphene contained a large amount of SDS-based surfactants. The insulating SDS residues can deleteriously affect the electrical properties by hindering the nanotube junction resistance. To enhance the nanotube junction resistance, nitric acid was introduced, and very effective removal of surfactants was observed, which enhanced electrical properties by improving better contact between each SWCNTs.
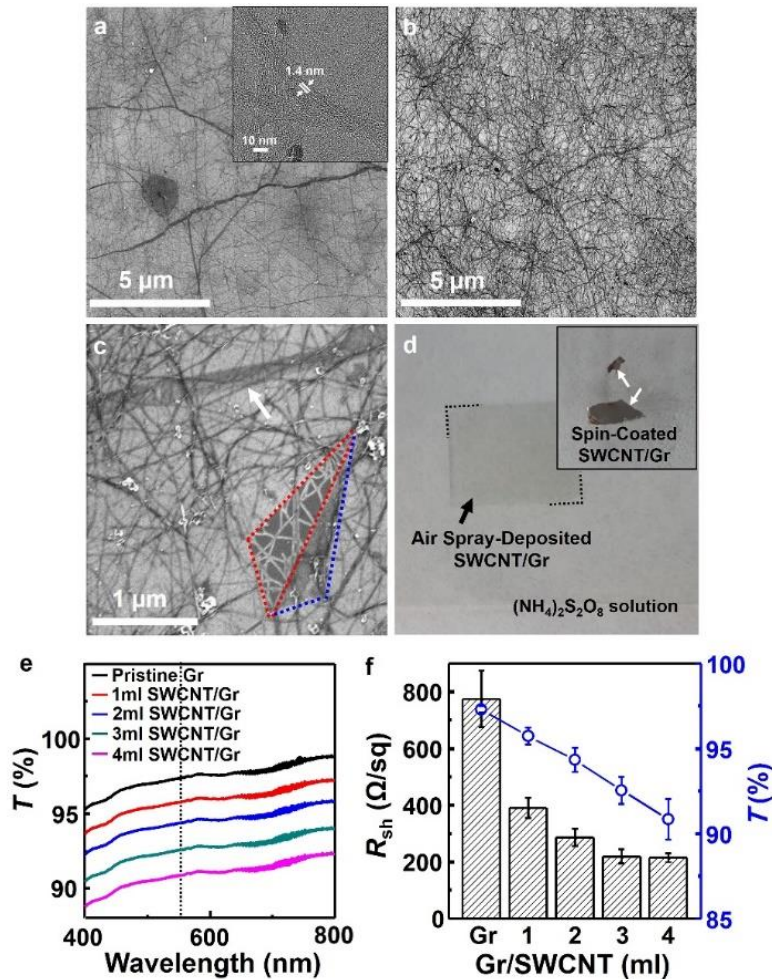
Figure 2-4. (a-b) A surface image of SWCNT/graphene/PET composite by using a SEM. SWCNT solution was air-spray coated on a single layer graphene from a copper foil by varying (a) 1 ml and (b) 4 ml of the solution and transferred to a PET substrate. (c) A surface image of various defects on a single layer graphene by using a SEM. A white arrow indicates wrinkle formed on a single layer of graphene. (d) A photo image of sacrificial polymer free-SWCNT/graphene composite floating on a copper etchant solution. The inset photo image presents inhomogeneous SWCNTs spin-coated on a graphene. The composite was torn apart on a copper etchant solution. (e) Transmittances of graphene/PET and SWCNT/graphene/PET composites at visible ranges. (f) opto-electrical data of SWCNT/graphene/PET composite by varying SWCNT solution.

2.4.3 Mechanical Properties of Graphene and Single-walled Carbon Nanotube/Graphene Hybrid Composite

The flexible and wearable electronic application requires TCEs materials to present high mechanical strength under certain strains. The flexible TCEs bust resistance under high bending, stretching, or even at twisting conditions. To study the mechanical property of our SWCNT/graphene and graphene composite film, the bending study was evaluated with a home-made resistance sensing based bending tester. As demonstrated by Figure 2-5a, the pristine graphene/PET composite showed sensitive resistance changes to bending. When bending radius of ~6.7 mm was applied, the sharp increase of resistance changes was observed. In contrast, when SWCNTs were uniformly coated on the graphene/PET composite by using the air spray deposition method, highly stable resistance was observed upon bending when SWCNT solution amounts were increased over 3 ml. For example, 237 % of resistance increment was observed at a bending radius of 2.7 mm for pristine graphene/PET composite. However, small decrement of resistance changes (6 %) was observed for SWCNT (4 ml)/graphene/PET composite. This was attributed to the uniform coating of SWCNTs, and reinforced single layer graphene under tensile strength by retaining their uniform networks in π-π stacked structure of SWCNT/graphene composite. Figure 2-5b shows the resistance changes as a function of bending cycle. Each composite was bent for 2,000 cycles at a bending radius of 2.5 mm and linear resistance change was recorded in real time. The larger increment in linear resistance was observed for pristine graphene/PET composite. In contrast, lower resistance change for SWCNT/graphene composite was observed. All composites presented linear increment of resistance during bending; however, the change of linear resistance under constant 2,000 bending cycles of (ΔR) was only 1.7 % for the SWCNT (4 ml)/graphene/PET film but 9 % for the pristine graphene/PET. where $\Delta R = (R_f - R_i) / R_i$. ($R_f$: final resistance value, R_i: initial resistance value). Since SWCNT/graphene/PET composite showed stable resistance changes under bending, the composite was fabricated as strain sensor to demonstrate as a wearable device application. Figure 2-5c demonstrates a strain sensor fabricated by using a SWCNT/graphene/PET composite in a human finger (effective bending radii: ~4 mm). The strain sensor produced electrical signals when the index finger bends or extends. The SWCNT/graphene/PET composite expressed stable electrical properties under bending condition, and a highly reproducible resistance change was obtained during finger actions. The origin of the large differences in mechanical and electrical stabilities of the pristine single layer graphene and the SWCNT/graphene composite on PET under loads was investigated by analysing the surface morphologies of pristine graphene/PET and SWCNT/graphene/PET composites after performing bending cycles between 100 and 2,000 times at a bending radius of 2.5 mm. As indicated in Figure 2-5d-e, clear white strip lines (indicated by white arrows) perpendicular to the bending direction was observed after bending the pristine graphene/PET composite. When bending cycles increased from 100 to 500, the widths and densities of the white strip

lines increased significantly. We assumed same phenomenon would have happened on the SWCNT/graphene/PET composite if the white strip lines were grooves in the PET origin from the deformation upon bending; however, white strip lines were barely generated on the SWCNT/graphene/PET composite even after bending the composite film more than 1,000 times (Figure 2-5f-g). This implies that the white strip lines are the line defects generated in the graphene layer during bending. According to the mechanical property analysis result, we believe that the SWCNT incorporation with graphene/PET composite is effective for inhibiting the defects formation in the graphene layer under various strain, resulting in the enhancement of mechanical and electrical stabilities.
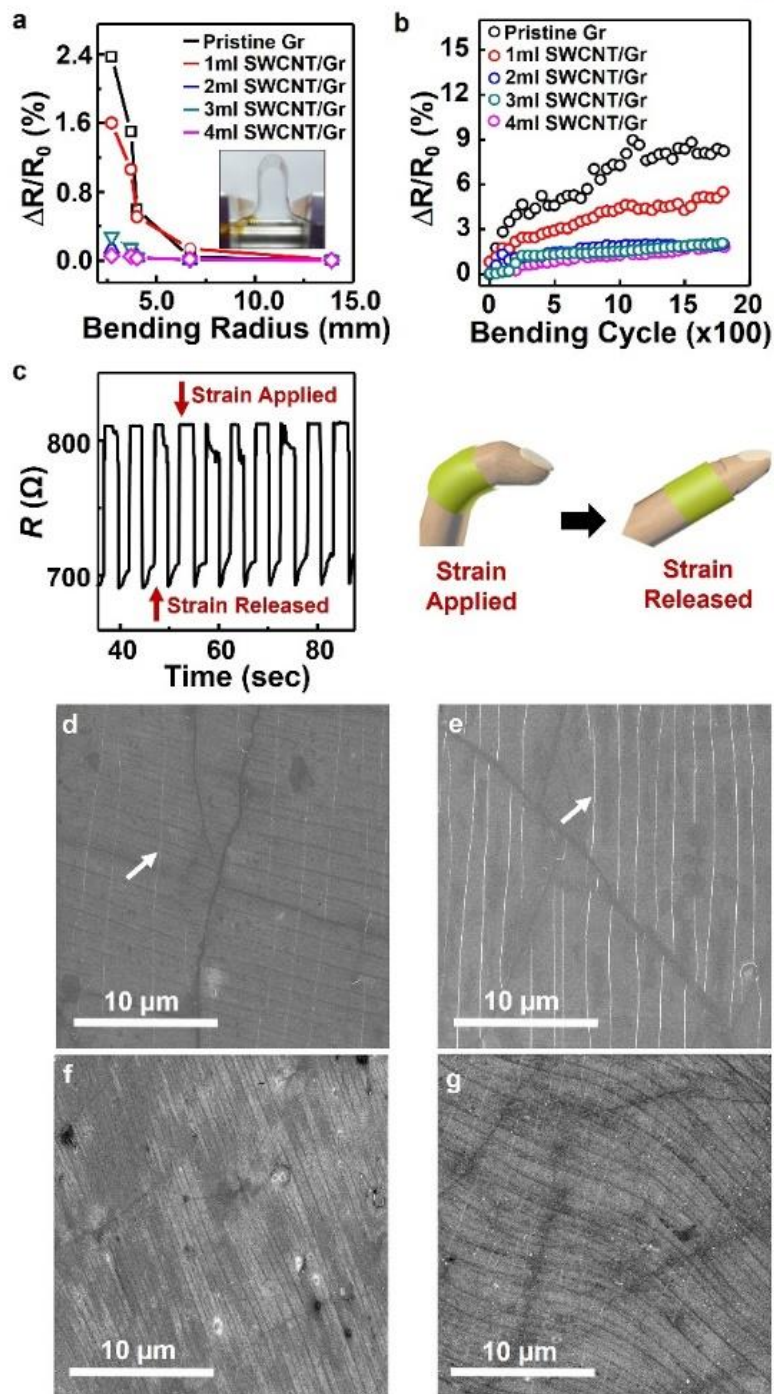
Figure 2-5. (a) Bending study and analysis of single layer graphene/PET and SWCNT/graphene/PET composite was performed by using homemade bending analyzer at various bending radii. (b) Electrical resistance changes of single layer graphene/PET and SWCNT/graphene/PET composites as a function of bending cycles at a 2.5 mm bending radius, (c) Smart bandage wearable sensor fabricated by SWCNT (4 ml)/graphene composite film attached on a human finger as a function of time. (d,e) SEM images of single layer graphene/PET composite bent at (d) 100 and (e) 500 times. (f,g) SEM images of SWCNT (1 ml)/graphene/PET composite bent at (f) 1000 and (g) 2000 times.

2.5 Doping Methods for Graphene and SWCNT/Graphene Hybrid Composite

2.5.1. Chemical doping of graphene films.

Various defects on graphene significantly hinder its property. In addition, graphene is known as a semi-metal which band-gap does not exist. Thus, many researches have put large efforts to enhance graphene property by doping to modify its electronic properties. To enhance the electrical property of graphene films, Fermi level of graphene's zero-gap band structure must be shifted away from the Dirac point by adjusting the carrier concentration of the graphene layer. The shift of Fermi level can be performed by various methods such as chemical doping[48], electrostatic gating[49], or a metal contact[50], resulting in the modification of graphene electrical performance. For instance, electron (n) or hole (p) doping can be obtained by incorporating other atoms such as boron or nitrogen. During graphene growth, such foreign atoms can be directly inserted into the carbon lattice. Typically, N-doped graphene are formed during the growth of graphene at in-plane edges or defective sites of graphene because they are more chemically active than less defective plane of graphene[51]. Similarly, B-doped graphene are formed at in-plane edges or defective sites by B-C bond and B-O bond[52]. Doped graphene can also be obtained through the molecular adsorption on its surface. For instance, treatment of $AuCl_3$ solution, $AgNO_3$ solution, Au and Ag particles can be generated on the surface of the graphene layer by the continuous reduction of metal ions (hole doping process), which may up-shift in the surface potential and electrical performance. Nitric acid (HNO_3) doping is another example of a molecular adsorbate that can be introduced for effective p-doping on graphene layers[53].

2.5.2 Opto-electronic Property of $AuCl_3$ doped Graphene, and SWCNT/Graphene composites

To achieve electrical property of graphene for industrial criteria TCEs, sheet resistance $\leq$ 100 ohm/sq and transmittance $\geq$ 90 % at visible range must be obtained. Opto-electronic property of pristine graphene/PET and SWCNT/graphene/PET composites were enhanced significantly by introducing the $AuCl_3$ solution for chemical doping. The doping process was performed by treating the composites with 20 mM of $AuCl_3$ dissolved in nitromethane solvent, which was then spin-coated on the graphene/PET or SWCNT/graphene/PET composites at 3,000 rpm for 30 seconds. Figure 2-6a presents chemically doped composites after spin-coating of $AuCl_3$. The sheet resistance of the SWCNT/graphene composite coated with 1, 2, 3, and 4 ml of SWCNT solution was reduced to 140 ± 47, 133 ± 21, 107 ± 12, and 105 ± 15 ohm/sq while showing only 1 % of transmittance decrement at visible ranges, respectively, in conjunction with enhanced carrier densities in all samples compared to the undoped samples. The enhancement in the sheet resistance was attributed to the fact that $AuCl_3$ got reduced by the electrons transferred from the 2-dimension hybrid carbon film due to the large reduction potential difference

between $AuCl_3$ and graphene (or SWCNTs), resulting in the positively charged 2-dimension carbon film, as reported in many literatures.
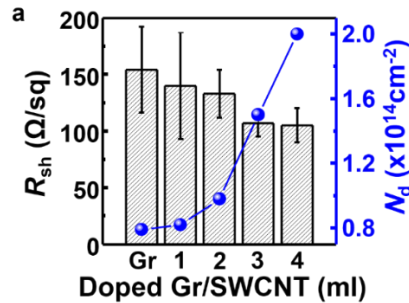
Figure 2-6. (a) Evaluation of sheet resistance and carrier densities of $AuCl_3$ doped SWCNT/graphene/PET composites by varying SWCNT amount solution.

2.5.3 Raman Spectroscopy and TEM Analysis of doped graphene and graphene/SWCNT composites

The hole doping process by introducing $AuCl_3$ doping solution on a carbon composite blue shifted the G band of graphene/PET or SWCNT/graphene/PET composites via the phonon hardening phenomenon in the Raman spectrum (Figure 2-7a). In addition, reduced Au nanoparticles from Au^{3+} on the SWCNT/graphene composite film were observed by SEM (Figure 2-7b). We noted that Au nanoparticles were formed along with side walls and junctions of each SWCNTs, resulting in the enhancement of electrical properties in the $AuCl_3$ doped SWCNT/graphene/PET composite. The intercalation of Au nanoparticles may have gradually reduced contact resistance between each SWCNT strands. This indicates that there are more chances to enhance opto-electronic properties of the SWCNT/graphene based TCEs by optimizing the physical and chemical properties of graphene during and after growth process.
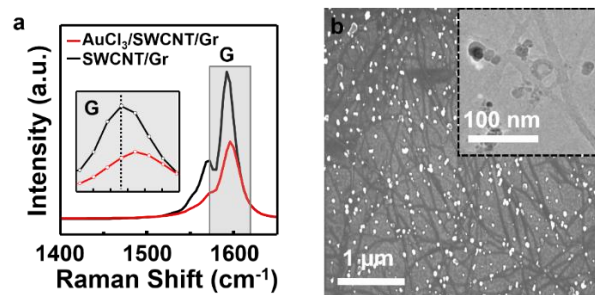
Figure. 2-7 (a) Raman spectra of SWCNT/graphene/PET composite and $AuCl_3$ doped SWCNT/graphene/PET composites. (b) SEM images of $AuCl_3$ doped SWCNT/graphene/PET composite. An inset image indicates gold nanoparticles intercalated in between each SWCNT bundles.

2.5.4 Thermal Stability of doped Graphene and SWCNT/Graphene Hybrid Composite and X-ray Photoelectron Spectroscopy Analysis

Previous studies have showed that the chemical doping of SWCNTs or graphene can significantly improve the opto-electrical properties. However, chemical doping of carbon materials is unstable because of easily desorbing dopant under mild temperature and ambient conditions. Thus, we analyzed thermal stability of chemically doped graphene/PET or SWCNT/graphene composites by measuring the sheet resistance changes under different temperatures at 50, 100, and 150 ˚C for 30 min(Figure 2-8a). It is noted that no significant changes were observed when composites were left at temperature under 100 ˚C; however, the sheet resistance of $AuCl_3$ doped graphene and graphene/SWCNT composite was significantly increased upon annealing at 150 ˚C. The sheet resistance of $AuCl_3$ doped graphene was increased by 155 % when compared to the composite before heating. In contrast, $AuCl_3$ doped SWCNT (4 ml)/graphene composite only showed 25 % increment of sheet resistance after heating. This strongly indicate that $AuCl_3$ doped SWCNT/graphene composite possess higher thermal stability than $AuCl_3$ doped graphene/PET substrate. The XPS study was performed to analyze the enhanced thermal stability of $AuCl_3$ doped SWCNT/graphene composite by studying the modified chemical states in the remaining dopants from $AuCl_3$ after heat treatment at different temperature. Here, the normalized intensity as the ratio of intensity was defined at given temperature with respect to intensity obtained at room temperature. As indicated by Figure 2-8b-c, the normalized intensity of Au^{3+} peaks in $AuCl_3$ doped graphene/PET composite was diminished and the Cl^- peaks almost disappear when composite was treated at 150 °C for 30 min (left panels in b,c). In contrast, $AuCl_3$ doped SWCNT/graphene composite showed large amounts of dopant (Au^{3+} and $Cl^{-)}$ still retained after heating process. This indicate that charge transfer from dopants are more stable and strongly adsorbed on the SWCNT/graphene composite. From inset image of Figure 2-7b, it can be noted that SWCNT networks are assembled by individual tubes and provide many interstitial sites such as vacant spaces centered in the triangular-shaped nanotubes or groove sites. These sites may provide higher attractive potential energy than the flat graphene surface. Therefore, enhanced binding energy at such sites with higher specific area can improve the thermal stability of chemically doped SWCNT/graphene composite.
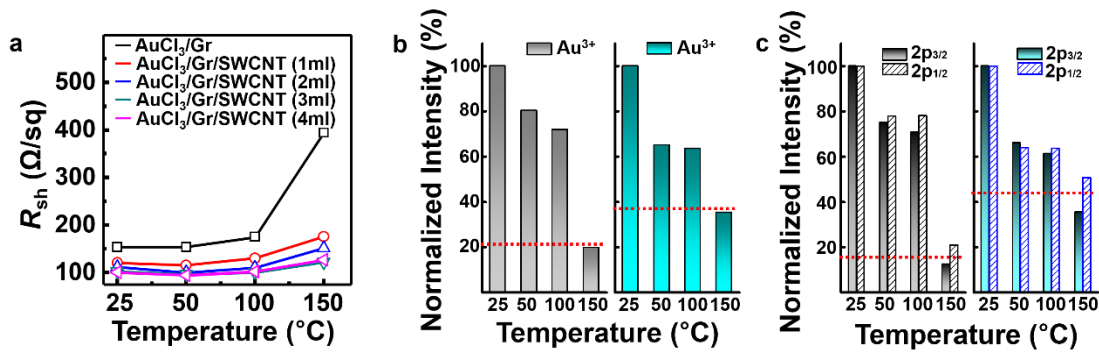
Figure 2-8. (a) Thermal stability evaluation of $AuCl_3$ doped single layer graphene/PET and SWCNT/graphene/PET composites. (b,c) The XPS analysis of normalized intensities of (b) Au^{3+} and (c) Cl^- $2p_{3/2}$, Cl $2p_{1/2}$ peaks in XPS spectra of $AuCl_3$ doped, graphene/PET (left panels) and SWCNT/graphene/PET composites (right panels) by varying annealing temperatures.

2.6 Conclusion

High performance and bending durable SWCNT/graphene composite based TCE was fabricated by facile air-spray coating of SWCNTs solution on a copper/graphene assembly followed by wet-transfer process to a transparent PET film. By studying and optimizing the CNT coating technique, the SWCNT/graphene composite based TCE performance including optoelectronic properties, mechanical durability, and thermal/electrical stability were enhanced significantly. It was presented that the SWCNT/graphene composite provide most effective form of TCEs, compared to CVD grown single layer graphene or SWCNT only films. The observation of the as-prepared SWCNT/graphene composite based TCEs after numerous bending study indicates that the SWCNT/graphene composite based TCEs exhibited excellent bending durability and electrical properties. In addition, we believe that further enhancement of such properties can be improved by incorporating metallic or higher aspect ratio SWCNTs.

Chapter 3. Modified Polyol Synthesis of Silver Nanowire by Using Continuous Flow Method

3.1 Introduction

Highly conducting 1-dimension nano-materials have received great attentions due to its increasing demands for plastic electronics in displays, touch screens, solar cells, and light emitting diodes (OLEDs) with addition to their excellent optoelectronic, catalytic, and flexible properties. Unlike indium tin oxide (ITO), highly conducting 1-dimension metal nano-materials exhibit high flexibility thus providing various applications for flexible transparent conducting electrodes (TCEs). Although ITO exhibit excellent optoelectronic properties, its growing cost and poor mechanical property limits its potentialities toward to future applications. Many attempts were made to replace ITO, for example, carbon nanotubes/fibres, metal wires, highly conducting polymer, high quality graphene, and metal grids were introduced for various applications. However, trade-off characteristic between optical and electrical property does not match up with commercial demands for transparent conducting electrodes (TCE). Among many alternatives, silver nanowire (AgNW) is one of the most promising material that can replace ITO, because they have very high ratio of DC conductivity to optical conductivity, requires simple fabrication process with environment-friendly solution-based synthesis method, and easy to scale up for various industry applications. Numerous AgNW synthesis methods have already been reported such as; hydrothermal[54], microwave-assistance[55], photo-inducted[56], and polyol method[57]. However, most of the silver nanowires in now days are synthesized by using a polyol method due to its simple and high-quality production. Yet, the sensitive experimental condition of AgNW synthesis limits polyol method to batch production. Although high aspect ratio of AgNWs by using a polyol method was reported by several research groups, their reaction time is often too long, and require very high reaction temperature (> 200 ˚C). Some studies insist that polyol synthesis of AgNWs can also be affected by adjusting the stirring speed of magnetic bar which can influence the reaction kinetics by changing the local concentration of Ag ions or break the AgNWs due to the shearing force[58]. Since conventional polyol method of AgNW synthesis is highly sensitive for stable and uniform synthesis of AgNWs, it is necessary to develop an efficient way to obtain high quality AgNWs. Micro and milli fluidic synthesis methods are very useful to prepare 0-dimension, and 1-dimension nanomaterials[59]. By utilizing the fluidic synthesis method, it can offer several benefits when compared with macroscale chemical reactors such as; in-situ real time reaction monitoring, rapid screening of parameters, low chemical use during reaction condition optimization, enhanced heat transfer and reproducibility. Recently, Gottesman et. al. introduced microfluidics to apply continuous flow method for AgNW synthesis[60] and Chou et. al. demonstrated AgNW synthesis by using a continuous flow method by

introducing a tubular glass coil[61]. Although few AgNW synthesis methods by using a continuous flow method were reported, most of the AgNW products lack in high aspect ratio and selectivity. In this study, we demonstrated one-pot synthesis of AgNWs by using a continuous flow method. High aspect ratio AgNWs (~ 30 µm in length, ~ 25 nm in diameter, and an aspect ratio of 800) were obtained by using PVP (polyvinylpyrrolidone), NaCl (sodium chloride), and NaBr (Sodium bromide) as the capping and seeding agents. Compared to other reports, our method requires very short reaction time (11.5 min), at a moderate reaction temperature (160 ˚C) for AgNW synthesis. With help of sedimentation assisted recovery method, high purity AgNWs were obtained and applied to fabricate TCE (transparent conducting electrode) and wearable devices which show a low sheet resistance of 23 Ω/sq and high transmittance of 94.5 % at 550 nm and exhibit highly stable resistance upon stretching when incorporated with silver nanoparticles (AgNPs).

3.1.1 Mechanism of Polyol Synthesis of Silver Nanowires

Various nanostructure can be fabricated by "polyol" method which is generally applied to synthesis various metal nanoparticles and nanowires. At the initial stage of AgNW synthesis, heating silver ions with ethylene glycol and capping agent will help silver particles to grow into various Ag nano-structure. During reduction of Ag^+, homogeneous nucleated AgNPs are well dispersed in organic solvent with help of a polymeric surfactant PVP which could act as steric hindrance and chemically adsorbed onto the surfaces of Ag through O–Ag bonding[62]. PVP has a strong affinity on various chemicals to form coordinative compounds due to the strong polar group from polyvinyl skeleton (pyrrolidone ring). The C=O polar groups in PVP interact with Ag^+ ions and form coordinating complex. When the dispersion of AgNPs is continuously heated at 160 °C, the small nanoparticles progressively disappears to form larger one via the Ostwald ripening process. PVP which is a structural directing agent, adsorb onto specific sites of Ag nanoparticle and to grow into rod-shaped structures. The growth process would continue until all the AgNPs were completely consumed and only nanowires survived. Addition of seeding particles by introducing metal halide such as sodium bromide (NaBr), sodium chloride (NaCl), copper chloride (CuCl), iron chloride ($FeCl_3$) also helps to grow AgNWs with high aspect ratio[63]. Typically, the high concentration of Ag^+ ions in the reaction solution can cause various structure formation of Ag. However, by adding metal halide, (i.e. CuCl, NaCl), the high Cl^- concentrations induce $M•Cl_2$ formation and effectively reduce the free Ag^+ concentration in the reaction system by generating AgCl. Subsequently, slow release of Ag^+ will also contribute high-yield generation of the multiply twinned Ag seed which is thermodynamically more stable for growth of AgNWs. When enough number of multiple twinned form the nanoparticles, the PVP associates and bind preferentially. This selective bind of PVP result in 1-dimension growth of fivefold twinned nanowires.

3.2 Experiment

3.2.1 Polyol Synthesis of Silver Nanowires by Using Continuous Flow in a Capillary Tube

Here, we synthesized AgNWs by using a continuous flow method with home-made glass tubular reactor (Figure 3-1). The chemical agents used are as follow: Silver naitrate (AgNO$_3$ ≥ 99.0 %), sodium chloride (NaCl, ≥ 99.0 %), sodium bromide (NaBr, ≥ 99.0 %), polyvinylpyrrolidone (PVP, MW: 360,000), and ethylene glycol (EG, anhydrous, 99.8 %) were purchased from Sigma Aldrich and used without further purification. An ammonia water (25-30 %) was purchased from Junsei Chemical Co., Ltd. In brief, AgNWs were synthesized by using a modified polyol synthesis method. First, 1.008 g of PVP was dissolved in 30 ml of EG. Separately, two sets of seeding solutions (NaCl and NaBr) were prepared at molar concentration ranging from 0.1 to 2.0 mM). After complete dissolution of PVP in an EG solvent, an appropriate amount of seeding solutions was added and well mixed for an hour at room temperature. Next, 0.509 g of AgNO$_3$ was dissolved in an EG solution containing PVP, NaCl, and NaBr, for 10 min at room temperature. The obtained mixture solution is transferred to a glass syringe and the solution was inserted to a continuous flow reactor by using a syringe pump for AgNW synthesis. The temperature of a continuous flow reactor was set at 160 ˚C and the retention time was precisely controlled by adjusting the syringe pump injection speed.
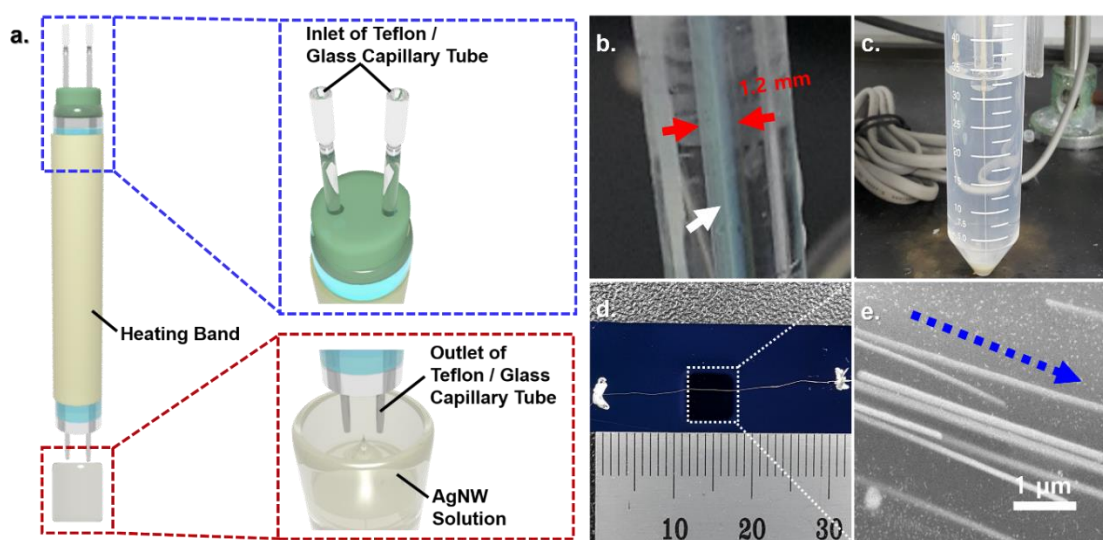
Figure 3-1. (a) A schematic illustration of AgNW synthesis by using a continuous flow method. (b) A photo image of AgNW reaction solution passing through a capillary tube. The inner diameter of capillary tube is 1.2 mm. A white arrow indicates synthesis of silver structure during flowing the solution. (c) A photo image of AgNW solution recovered through outlet of a capillary tube. (d) A photo image of AgNWs wrapped with PVP after the acetone treatment. (e) A SEM image of AgNWs wrapped with PVP after the acetone treatment. A blue arrow indicates AgNWs arrayed in to one direction.

3.2.2 Relationship Between Molar Ratio of Polyvinyl pyrrolidone and AgNO₃, and seeding condition

By using a solution-phase method, various metals can be synthesized into monodisperse nanoparticles with specific compositions and structures in large amounts. Despite this, controlling shape of metal nanoparticles is very difficult. In general, most of the face centered cubic (FCC) structure metal nanoparticles tend to grow into multiply twinned structure with surfaces bounded by the lowest energy {111} facet. Other less stable structures and shapes of metal nanoparticles are generally obtained by adding chemical structure directing agents (capping agents) during the synthesis. There are reports that addition of PVP during the metal nanoparticle growth reaction effectively passivate (100) faces of the multiply twinned particles and leave (111) planes active for nanowire growth at [100] direction[64]. During nanowire growth, Ag^+ ions are continuously supplied and with help of PVP, multiply twinned particles eventually grow into Ag nanowires. Thus, it is very important to optimize molar ratio of PVP to $AgNO_3$ for obtaining high aspect ratio of AgNWs. It has been reported that such optimization of molar ratio between PVP to $AgNO_3$ is very effective for controlling selectivity of AgNWs from AgNPs with addition to controlling the aspect ratio[65]. For instance, when the molar ratio of PVP:$AgNO_3$ is too low, the passivation of {100} faces of MTP is not enough which lead to growth of Ag nanostructure on both {111} and {100} faces. This result in growth of AgNWs with large diameters. In addition, the multiply twinned particles that failed to grow into nanowires aggregate and generates large quantity of nanoparticles. In contrast, when the molar ratio of PVP:$AgNO_3$ is excessively added, very thin AgNWs are obtained. However, too much PVP can passivate all surface of AgNPs, and inhibit the growth of AgNWs. Thus, it is very important to optimize molar ratio of PVP:$AgNO_3$ for AgNW growth. If there are too much of free Ag^+ in the reaction system, various structure of AgNPs can be generated instead of obtaining Ag MTPs. This issue can be controlled by addition of metal halide. Introduction of seeds can effectively alter the nucleation process at the beginning stage of AgNW growth. There are many reports on AgNWs synthesis by using various nucleation agents. Typically, chlorine-based salts exhibit good results, and in particular NaCl is one of the mostly used salts. When there are nucleating agents in the reaction system, it affects the morphology of metallic seeds. In addition, NaCl in the system reacts with Ag^+ to form AgCl nanostructure and reduces the free cationic silver ion concentration during initial seed formation. This result in slow reaction speed and enables the generation of more thermodynamically stable multiply-twinned Ag seeds which is required for nanowire growth[66]. In our system, control of molar ratio between PVP to $AgNO_3$ did little effect on the growth of AgNWs in continuous flow system. As shown in the Figure 3-2, molar ratio of PVP to $AgNO_3$ was modified and negligible difference was observed. Large quantity of AgNWs and AgNPs were observed together with almost every condition. Yet, direct evidence for such phenomena is lacking, it is believed that Ag MTP is not efficiently obtained when only PVP and $AgNO_3$ condition was modified in the system. It can be

assumed that since milli-fluidic reaction system is effective for heat transfer, reaction speed was too much fast inducing amorphous AgNPs generation. By collecting AgNWs only, it was found out that when molar ratio of PVP to AgNO$_3$ was 3, highest aspect ratio of AgNWs were obtained.
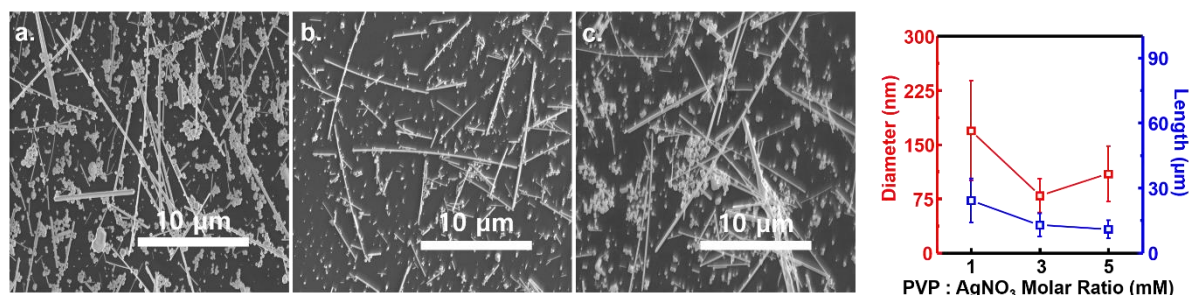
Figure 3-2. (a-c) SEM images of AgNW synthesized by varying molar ratio of PVP:AgNO$_3$. Molar ratio of 1, 3, 5 was used for AgNW synthesis respectively. (d) Length and diameter data of AgNWs by varying molar ratio of PVP to AgNO$_3$

  Based on this condition, addition of metal halide method for seed was introduced to enhance the Ag MTP yield. Previously, various kinds of seeding reagent (for example, NaBr, FeCl$_3$, AgCl, NaBr, and KBr) were studied for AgNW growth. The formation of AgX (X=Br, Cl) can reduce the concentration of free Ag$^+$ in the solution and increase the Ag MTPs which is thermodynamically more stable. Figure 3-3. represent a trend of AgNW length and diameter by varying the various seeding condition. When NaCl was introduced in the reaction system, large amount of AgNWs were obtained rather than AgNPs with 54.5 ± 28.53 nm and 19.65 ± 6.22 µm of diameter and length respectively. Conversely, highest silver products including AgNWs and AgNPs were obtained when NaBr was introduced in the reaction system with 30.73 ± 8.67 nm and 14.05 ± 7.21 µm of diameter and length respectively. In our reaction system, AgNW was the major product when Cl$^-$ introduced for growth of AgNWs; however, Br$^-$ worked better to reduce the diameter of the AgNWs. When Cl$^-$ was introduced in the reaction system, it can react with Ag$^+$ to form AgCl and reduce the concentration of free Ag$^+$ in the solution to generate Ag MTPs that can grow into AgNWs. However, large quantity of tiny Ag nucleus was generated when Br$^-$ was introduced in the reaction system. Yet, there are no clear evidence for such phenomenon, but previous reports stat that introduction of AgBr can enhance the reaction rate speed enormously. Although very tiny multiply twinned seed particles are generated which eventually became very narrow AgNWs, unstable small multiply twinned particles may transform into other shape particles via fluctuation before growing into nanowires.
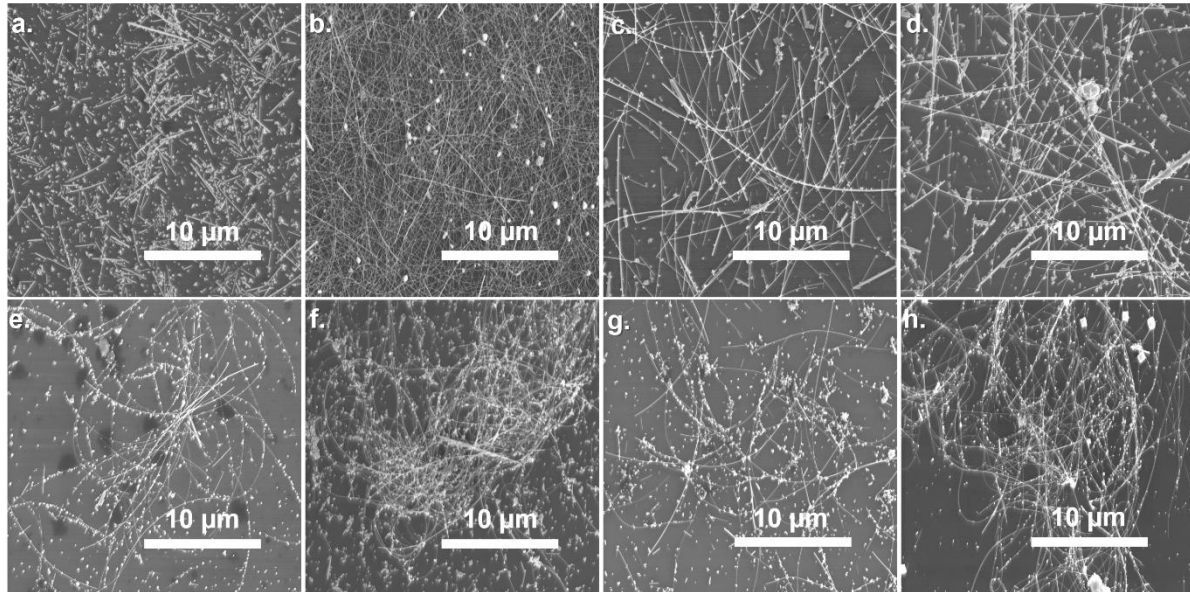
Figure 3-3. (a-d) SEM images of AgNW synthesized by varying molar concentration of NaCl 0.1, 0.5, 1.0, and 2.0 mM respectively. (e-h) SEM images of AgNW synthesized by varying molar concentration of NaBr 0.1, 0.5, 1.0, and 2.0 mM respectively.

Accordingly, NaBr and NaCl were used together to obtain thin AgNWs by optimizing the appropriate level of nucleation rate. Figure 3-4 shows AgNWs synthesized by using NaCl and NaBr seed together. NaCl molar concentration was fixed to 0.5 mM where major product of AgNWs were obtained, and molar concentration of NaBr was varied to optimize the reaction condition (0.1, 0.3, 0.5, and 1.0 mM). As it can be seen from Figure 3-4a-d, many nanoparticles were observed as the molar concentration of NaBr was increased. Although highest aspect ratio was achieved when molar concentration of NaBr was 0.1 mM, the standard deviation error was very large which could be misleading data. Thus, the optimized and highest aspect ratio seeding condition in this experiment was set to 0.5 mM of NaCl and NaBr, and AgNWs with length and diameter of 22.49 ± 6.13 nm and 18.0 ± 6.34 μm with an average aspect ratio of ~800 was obtained.
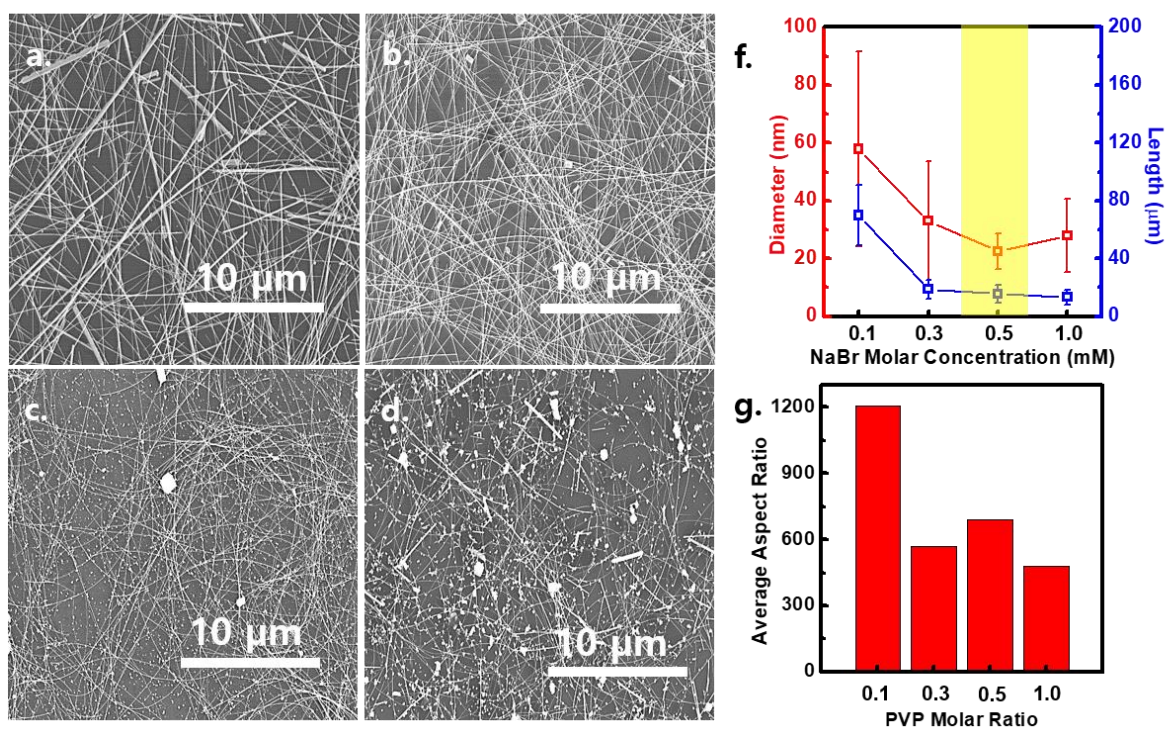
Figure 3-4. (a-d) SEM images of AgNW synthesized by varying molar concentration of NaBr 0.1, 0.3, 0.5, and 1.0 mM respectively. The molar concentration of NaCl was fixed to 0.5 mM. (f) Diameter and Length data of AgNWs. (g) Aspect ratio of AgNWs.

 With an optimized condition, reaction time study was performed by varying the reaction time at 6, 8, 9, 10.5, 11.5, and 15 min (Figure 3-5a-f). The reaction time was controlled by adjusting the syringe pump speed. It can be noted that at the beginning stage of the reaction (<6 min), most of the seed and nanoparticles were observed as an aggregated form; however, AgNWs started to appear when the reaction time passed 8 min. When the reaction time exceeded 15 min, overgrowth of AgNWs were observed. It is noted that optimized AgNWs were obtained with the reaction of 11.5 min which is well suitable for industry scale synthesis of AgNWs by using a continuous flow method. Stable and reproducibility is also very important for an industry scale synthesis of AgNWs. When a glass tube was used for AgNW reaction, large amount of silver mirroring was observed as reaction time elapsed. In addition, change in aspect ratio of AgNWs were observed as reaction continued from 0 to 30 min, indicating that non-uniform of AgNWs products were obtained (Figure 3-6a-b). Figure 3-7a-f shows reproducibility of AgNW synthesis by using a continuous flow method for up to 8 hours. Unlike a glass capillary tube, Teflon capillary tube can efficiently pass the solution during the reaction and prevent the silver mirroring effect on its wall. As it can be seen from Figure 3-7f. diameter and length distribution stayed similar although the AgNW production was continued up to 8 hours.
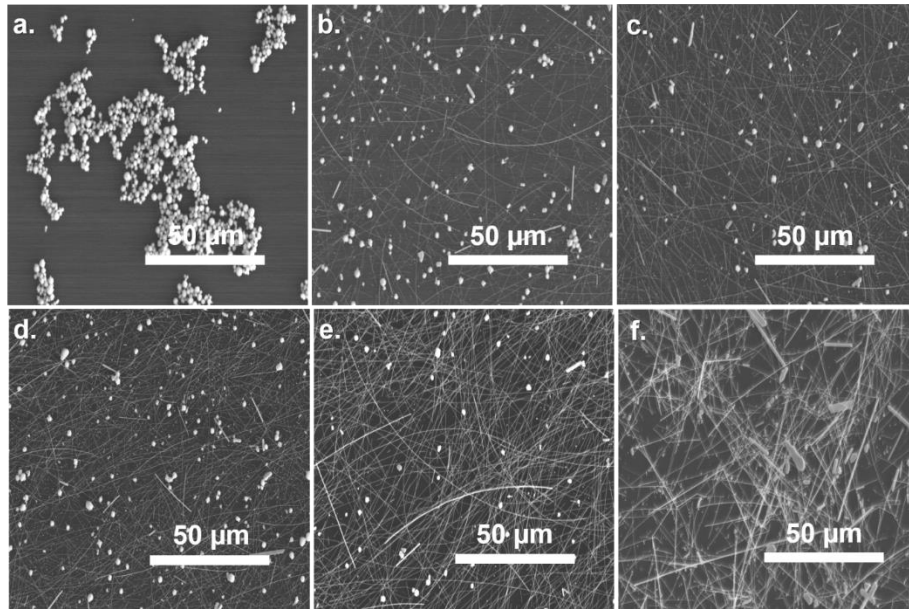
Figure 3-5. SEM images of AgNWs by varying reaction times (a) 6min, (b) 8 min, (c) 9 min, (d) 10 min 30 sec, (e) 11 min 30 sec, (f) 15 min
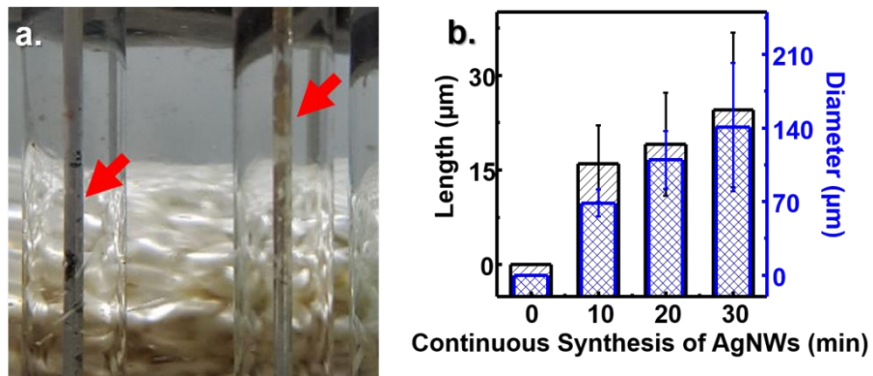
Figure. 3-6. (a) A photo image of AgNW synthesis by using a Teflon tube. Red arrows indicate silver mirroring during synthesis of AgNW by using a continuous flow method. (b) Length and diameter data of AgNW synthesis when glass capillary tube was used.
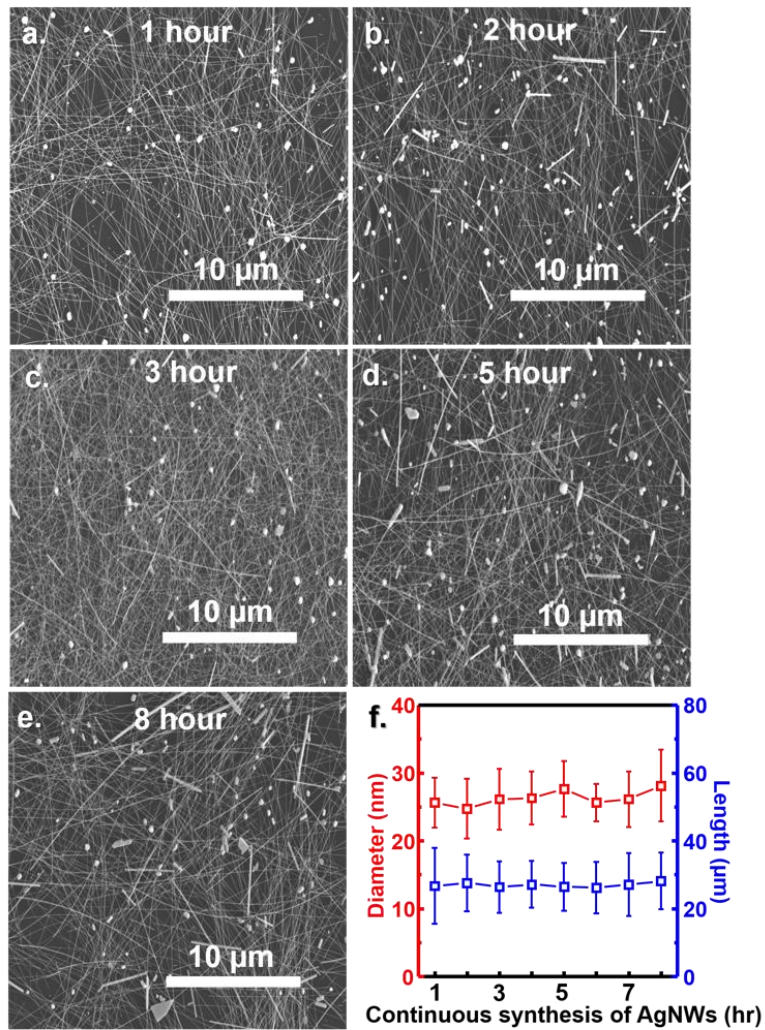
Figure 3-7. (a-e) SEM images of AgNWs coated on a Si/SiO$_2$ substrate. AgNWs were synthesized continuously by using a continuous flow method up to 8 hours. (f) Diameter and length data of AgNWs synthesized continuously by using a continuous flow method up to 8 hours.

3.3 Purification of Silver Nanowires

3.3.1 Silver Nanowire Purification Method and UV-visible Adsorption Analysis

When AgNWs are synthesized by using polyol methods, it is inevitably to avoid silver nanoparticles, small and thick silver nanorods as a side product. It is very important to selectively obtain highly pure AgNWs for practical applications. Conventionally, running numerous centrifugation cycles to separate AGNWs and side products was widely used. However, this process is time-consuming and sufficient purity of AgNWs were not obtained. Pradel and co-workers recognized a cross-flow filtration method to purify NWs; however, the yield of this method is highly dependent on many factors such as NW size, pore size of the fiber membrane, flow rate, and pressure, and lack in scalability. Thus, it is very important to develop a simple, convenient, and scalable method for separating nanoparticles from NWs. Here, we focused on the PVP adhered at the side wall of AgNWs. Since PVP is inevitably used for AgNW synthesis, it often contains small trace of PVP after AgNW synthesis is terminated. Since higher surface area for PVP adhesion is provided for AgNWs when compared with AgNPs, there are higher probability for AgNWs to settle at the bottom of the solution after time elapse. In addition, PVP is known for not soluble in acetone solvent. Thus, treating AgNW solution with acetone will accelerate AgNWs to settle at the bottom of the solution. In detail, when AgNW synthesis was completed, the AgNWs were purified by following steps: First, 5 ml of Ammonia solution was poured into a 15 ml of AgNW solution containing centrifugation tube. Then, acetone was slowly inserted with 5 ml steps until the small amount of floating precipitates were observed. As soon as the precipitates were observed, the solution was centrifuged at 500 rpm for 1 min. The aggregated AgNWs settled to the bottom of the centrifugation tube whereas, short AgNWs with nanoparticles were removed by pipet. The aggregated AgNWs were re-dispersed by adding 15 ml of distilled water containing 0.5 wt. % of PVP. Again, an acetone was slowly inserted with 5 ml steps until the small amount of floating precipitates were observed and centrifuged at 500 rpm for 1 min. The whole steps were repeated 5 times to obtain high purity AgNWs. As it can be seen from Figure 3-8a-d, as purification steps increased and reached 5 times, pure AgNWs without any AgNPs were obtained. It was also confirmed by a SPR spectrum, which is used widely to evaluate the size and shape of the AgNWs by studying the SPR bands that appear at different frequencies. The previous study has indicated that the main SPR signals for AgNWs with diameter ranging from 30-60 nm were observed between 372 and 380 nm. These peaks are known for the transverse mode of a 1D material with pentagonal cross sections, corresponding to out-of-plane quadrupole and dipole resonance modes. As it can be seen from Figure 3-9. the SPR absorption band clearly shifts to the lower wavelength as the purification process is repeated. This is due to the selective elimination of thick and small nanorods by the purification method proposed here (Figure 3-9a-b).
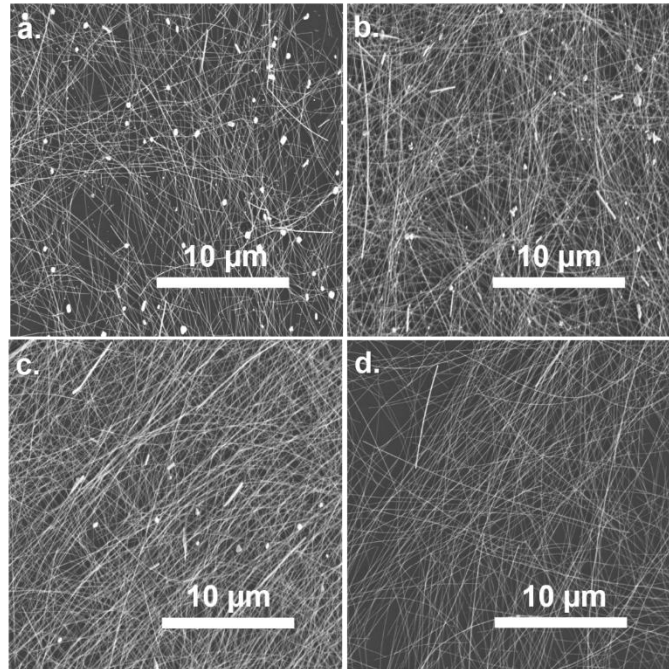
Figure 3-8. Purification of AgNWs by using non-solvent precipitation method. The AgNWs were purified (a) 0, (b) 1, (c) 3, and (d) 5 times

RSC. Adv., 5 (2015), p76092
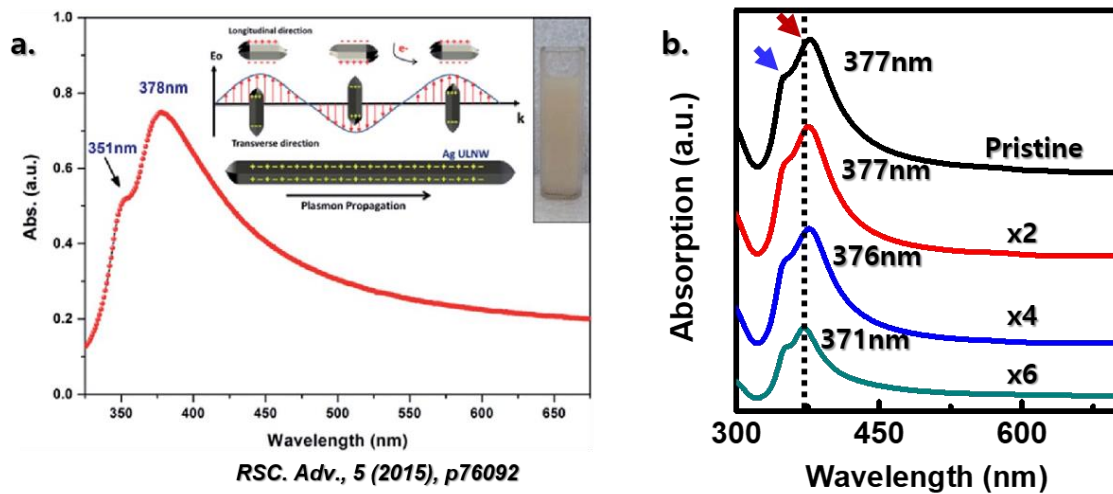
Figure 3-9. (a,b) UV-Vis absorption spectrum of AgNW solution.

3.4 Figure of Merits of Silver Nanowires Synthesized by Continuous Flow Method

3.4.1 Surface Characterization and Structure Analysis of Silver Nanowires by Using Scanning Electron Microscope and X-ray Photoelectron Spectroscope

  Generally, AgNW grows along [100] direction which exhibits a penta-twinned structure bound by five (100) planes and five triangular (111) facets joined at the tip which is shown in an inset SEM image of Figure 3-10 a. The lattice spacing of AgNWs was determined to be 0.238 nm, which agrees with the d value of the (111) plane of Ag (Figure 3-10b), and an inset image represent the Fourier patterns which corresponds to the single crystal with the FCC structure along the <100> zone axis direction. The FCC structure of AgNW was examined by X-ray diffraction (XRD) pattern. Figure 3-10c present XRD patterns and four diffraction peaks were assigned to (111), (200), (220), and (311) planes. The lattice constant calculated from the XRD pattern, according to the lattice spacing of the (111) planes are 4.102 Å, which is similar to the reported data value of 4.086 Å (A Joint Committee on Powder Diffraction Standards file No. 0-0783).
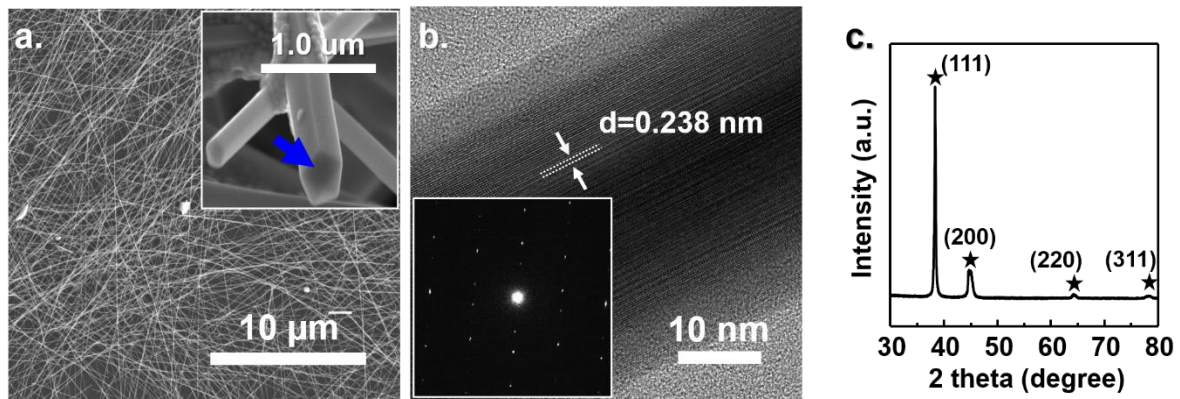
Figure 3-10. (a) A SEM iamge of AgNW networks spin coated on a Si/SiO$_2$ substrate. An inset image with a blue arrow indicates an AgNW with multiply twinned decahedral structure. (b) A HRTEM images of a silver nanowire. A white arrow indicate an AgNW was coated with PVP. (c) A XRD analysis of AgNW networks spin coated on a glass substrate.

3.4.2 Opto-electronic Properties of Silver Nanowire Coated Transparent Conducting Electrode

  The obtained AgNWs were dispersed in the mixture of IPA/distilled water at an optimized density of 0.3 mg/ml and spin coated on the Si/SiO$_2$ and polyethyl terephthalate (PET) substrate to examine its morphology. As it can be seen from SEM images in Figure 3-11a-d, high aspect ratio of AgNWs were well synthesized and coated on a Si/SiO$_2$ substrate. Since AgNWs were grown from Ag MTP seed, it

is also noted that the end of AgNWs had MTP structure. For uniform coating of AgNWs, the AgNW solution was spin-coated on a Si/SiO$_2$ and PET substrate for further investigation. AgNWs density can be uniformly coated on the substrate by increasing the number of coating from 1 to 4 times. It is noted that, high speed coating of AgNWs resulted in less AgNWs on a target substrate; however, low speed coating resulted in dense drop lets of solution residues which left coffee-ring effect and aggregation of AgNWs. In the experiment, we set the optimization AgNWs coating speed at 2000 rpm for 60 seconds. Changes in sheet resistance trade-off characteristic in PET substrate. As coating number increased, sheet resistance significantly dropped and showed saturation pattern after it exceeds two times coating number (Figure 3-11e). The transmittance characteristic was analyzed and showed the drop trend as the coating number increases (Figure 3-11f). It is noted that 29 ohm/sq and 94.5 % of transmittance at visible ranges were obtained which is comparable to ITO we use nowadays.
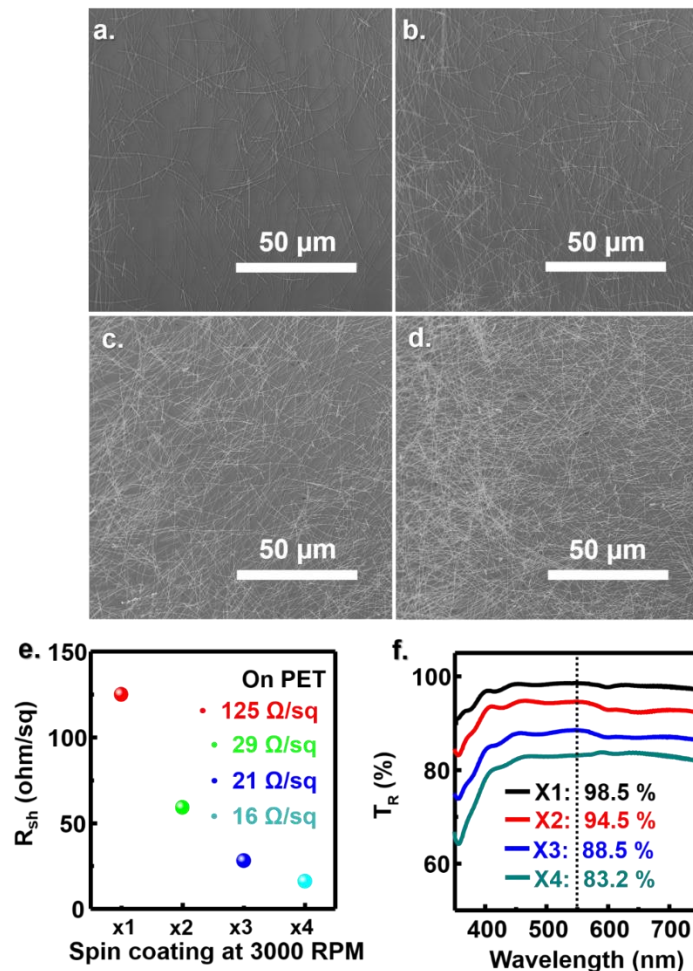
Figure 3-11. SEM images of purified AgNW solution (2 mg/ml) on a Si/SiO2 substrate spin-coated at 3000 rpm. The AgNWs were spin-coated (a) 1, (b) 2, (c) 3, and (d) 4 times. (e-f) Sheet resistance and transmittance data of AgNWs spin-coated on a PET transparent substrate with different number of coating.

3 4

3.5 Conclusion

High aspect ratio AgNWs were synthesized by using a continuous flow method. In contrast to conventional method, we obtained high quality AgNWs within 11.5 min, and the reaction was stable for more than 8 hours. In addition, high purity of AgNWs were obtained by purification method. By controlling precise volume ratio between acetone and PVP/distilled water solution, AgNWs were effectively separated from AgNPs by precipitation with a little help from low speed centrifugation. The optimized condition of AgNWs solution were spin-coated on a transparent substrate and 29 ohm/sq at transmittance of 90 % at visible range of wavelength was obtained. We believe that such continuous flow method has great potential for industry level scale fabrication of AgNWs and used for various applications that can replace ITO soon.

Chapter 4. Highly Stable Multilayer-Graphene/Silver Nanowires Composite Film with Colorless Polyimide Substrate for Opto-electronic Applications

4.1 Introduction

Development of technology is getting faster than before, people are requesting products they often watch in the science fiction. Size of transistors in a dense integrated circuit are gradually decreasing every year, and many electronic devices are getting smaller with better performance. In now days, we often talk about wearable devices with fifth generation mobile networks (5G) and expect facile communication between electronic devices to human. For such purpose, transparent conducting electrodes (TCEs) in display technology will get very important. In the past, the main issues for a TCE were electrical conductance and optical transparency at visible ranges. Substrate's rigidity, flexibility were not major issues since electronics such as television, cellular phone, and monitors did not require to be bent. However, big firms such as Samsung and Apple are producing electronic devices that has certain curvature in now days. Smart watch, curved TV and monitors are one of customers favorite. Another issue in TCE is a material stability. There are some cases where electronic device products must endure under harsh environment. Such harsh environment includes high temperature, high humid, or high impact conditions. For instance, batteries often get explosion when a running temperature of a device gets too high. Car batteries do not operate at low temperature. Smart windows may malfunction under humid day condition. Thus, achieving high electrical properties with high transmittance with addition to excellent mechanical properties and long-term stability are very important issues for an electronic device for future applications. In this chapter, flexible TCE with long-term stability will be discussed.

4.1.1 Performance of Various Transparent Conducting Electrodes

Emerging new materials for TCEs include of CNTs, graphene, conducting polymers, metal nanowires, and metal grids. Typically, TCEs in various applications must present sheet resistance of $R_{sh} < 100$ ohm/sq, with transmittance of $T > 90$ % in the visible ranges. For large-scale display, it requires better performance, such a sheet resistance must show $R_{sh} < 5$ ohm/sq. With excellent opto-electrical property of CNTs, it was proposed for next generation alternative TCE material. However, their potentiality is limited with high contact resistance from nanotube-nanotube contact. Thus, CNT is still far from practical applications. CVD grown graphene is another example of highly TC material for various TCEs applications. Among many graphene growth technique, CVD method is most applicable method to obtain large area, high crystalline graphene layers. The CVD method of graphene growth by using

transition metal catalyst (Ni and Cu) can produce high quality films when compared to graphene oxide. The CVD method of graphene is generally processed in a vacuum condition which is expensive than other deposition technique; however, a processing cost can be reduced when it is applied in industry scale production since low/high pressure CVD method is already being used in many current microelectronic industries. For instance, Kong's group and Hong's group reported graphene growth on a polycrystalline Ni film[67,68]. The graphene was transferred to a plastic or glass substrates by a wet-transfer method using sacrificial polymer layer such as PMMA or PDMS. These TCEs present 700-1,000 ohm/sq T=90 % and 280 ohm/sq T= 76 % respectively. For single layer graphene TCE grown from a copper foil often present better performance than the graphene obtained from nickel foil and exhibit (350 ohm/sq T= 90 %). Some report states that a four-layers of graphene (repeatedly transferred, p-doped) which exhibited 30 ohm/sq at T= 90 % can alternatively use to replace ITO. However, the excellent opto-electronic property of graphene can be only achieved through chemical doping, thus it is not suitable for TCEs in industry application. AgNWs can present high optoelectronic performance of 25-54 ohm/sq with 90 % of optical transparency[69]. Recently many researchers tried to improve electrical performance by introducing effective washing methods, or various welding methods. For instance, AgNWs can be simply welded together by treating with heat[70], Xenon lamp[71], laser[72] etc. There are reports of high-performance TCEs with hybrid structure of graphene and metallic nanowires. Despite to its high performance of AgNW based TCEs, long-term stability issue must be solved for practical applications.

4.1.2 Environmental Stabilities of Various Transparent Conducting Electrodes

CNTs and graphene are known for excellent inertness under various ambient conditions. They are stable at high temperature, high humidity, and acidic environments[73]. The high stabilities are attributed from CNTs and graphene possessing high crystalline structures with low defects. Thanks to long-term stability of CNTs and graphene, many electrical resistance-based sensors are demonstrated by using high crystalline carbon materials. It was reported that CVD graphene film transferred on a Si/SiO$_2$ substrate showed excellent stability of electrical conductivity under ambient conditions for 500 days[74]. Interaction between graphene and surrounding environments, such as oxygen, moisture and the substrate, could induce slight resistance changes (less than 10 %) of CVD graphene. Unlike highly stable carbon materials, AgNW stability is weaker than CNTs or graphene; it often gets sulfurized or oxidized under ambient condition. For high performance TCEs purpose, AgNWs are getting thinner than 100 nm in now days. Such small diameter can cause severe problems to instability and corrosion due to its high surface area to volume ratios. When AgNWs are exposed to air, they get disconnected when left in ambient conditions for less than 6 months which leads to electrode short. Humidity, high temperatures, light exposure, and electrical currents have all been found to accelerate AgNW

degradation[75]. As discussed earlier, several efforts were shown to enhance AgNWs stability significantly. For instance, AgNWs generally melt over 200 °C. It is reported that ZnO/MGO coating on AgNW networks via ALD process served efficiently as a protective layer from oxidation and detrimental process[76]. There are also report that coating of ZnO by using ALD process[77] allowing AgNW networks to withstand thermal process at 300 °C. Hybrid structure of graphene with AgNW networks are also reported by numerous groups. Ahn and Liang reported coating of reduced graphene oxide can provide excellent barrier films to prevent oxidation under high temperature and high humidity conditions[78,79]. Nam and Xu used CVD graphene as a barrier film for AgNW protection. They applied wet transfer method to transfer high crystalline single layer graphene on AgNW networks to prevent AgNWs from oxidation and sulfurization. Polymer coating (Teflon[80], and polyvinyl alcohol[81], or parylene C[82] was reported by Hu, Zhang, and Ahn, for barrier film on AgNWs. However, most of the research used expensive process method, or their barrier properties were not suitable for long-term stability for AgNW based TCEs.

4.1.3 Transparent Polyimide for High Performance Transparent Conducting Electrodes

There are various transparent polymer films used for fabrication of various optoelectronic devices. In recent of days, industry demand on optoelectronic devices is continuously increasing due to its high reliability, high transparency, and high integration. In addition, the transparent polymer films require higher temperature endurance property. For instance, one of the most favorably used display devices such as flexible thin-film transistor-based active matrix liquid crystal display (TFT-LCDs) or active matrix organic light-emitting display (AMOLEDs) requires fabrication process temperature on the flexible transparent polymer substrate over 300 °C. Current industry uses transparent polymer films which loses their transparency and mechanical properties when subjected into high temperature. Therefore, it is necessary to develop transparent and high temperature resistance polymer film for next generation display technology applications. Current transparent polymer films used widely in the industry can be classified with their glass transition temperature (T_g). Conventional transparent polymer films such as polyethylene terephthalate (PET, T_g: ~78 °C), or polyethylene naphthalate (PEN, T_g: ~123°C) exhibit T_g < ~150 °C; however, high-temperature transparent polymer films such as polycarbonate (PC, T_g < 148 °C) can possess ($100 \leq T_g < 200$ °C). There are polymer films that can endure at extremely high temperature $T_g \geq 200$ °C. Aromatic polyimide (PI) is known to present excellent thermal endurance property up to 300 °C. However, its application is optoelectronic device is limited due to deep yellow colors with poor optical transparency. Typically, PI can be synthesized by using two different methods. First method includes polyimide synthesis by using two steps. In the first general polyamic acid (PAA) method, dianhydride and diamine monomers will first polymerize in N,N-

dimethylacetamide (DMAc) to obtain PAA solution. The obtained PAA solution is sensitive to heat and moisture, which gets easily degraded at ambient condition. Coating PAA on a target substrate, and heat treatment from room temperature to elevated temperature allows it to get cured. This curing process evaporate solvents, but at the same time water molecules get removed which is often known as imidization process. Previous studies have reported that imidization process of PAA requires high temperature annealing (300-350 °C), which is necessary to completely transform PAA into PI. However, such process has deleterious effects. For example, high temperature can cause color of the PI films to become deep yellow. The second method includes soluble PI in organic solvents. For good solubility, flexible linkages (-O-, -CH$_2$-, etc.), or bulky substituents (alkyl groups, phenyl, etc.), and unconjugated structure (aliphatic or alicyclic groups) are added into the reaction system during synthesis of polyimide. These chemical additions can increase the solubility of PI resins in organic solvents and better for further processing.

4.2 Experiment

4.2.1 Synthesis of Transparent Polyimide by Melt-Polymerization Method

Here, we have developed facile and novel method for synthesis of PI. Conventional methods of PI synthesis often consume lots of time and requires numerous process steps (i.e. imidization of PAA). Instead, we have introduced melt-polymerization to obtain transparent and soluble PI powders. As it can be seen from the Figure 4-1, mixture of 4,4-(Hexafluroisopropylidene)Diphthalic Anhydride) and a,a'Bis(4-aminophenyl)-1,4-diisopropylbenzene) powders were put in an alumina boat with a molar ratio of 1:1. The mixture of each monomers in an alumina boat was put in a vacuum electro-furnace and annealed at 300 °C under low pressure vacuum for 1 hr. After melt-polymerization was over, fine yellow powders were recovered and collected for further analysis. As it can be seen from the Figure 4-2a-b, each monomers present glass transition temperature between 165 – 250 °C. Thus at 300 °C, melt-state monomers reacted together for PI synthesis. The melt-polymerized polyimide showed high resistance to thermal annealing, where it only presented 1 wt. % loss at 300 °C (Figure 4-2c). By using FT-IR analysis (Figure 4-2d), clear peak of imidization was observed indicating PI was obtained.
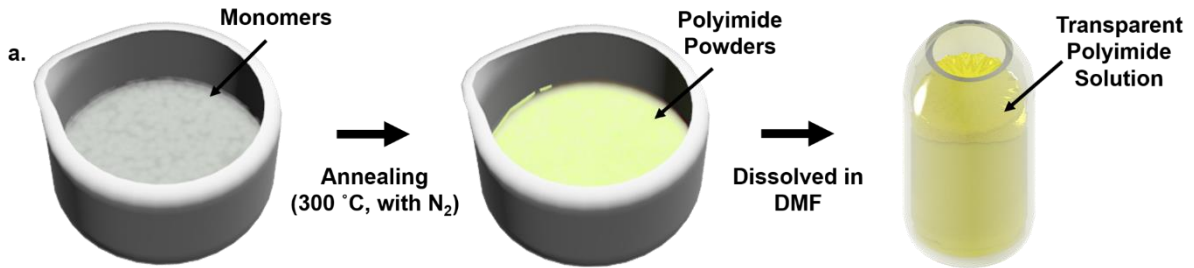
Figure 4-1. (a) A Schematics of polyimide synthesis method by using a melt-polymerization
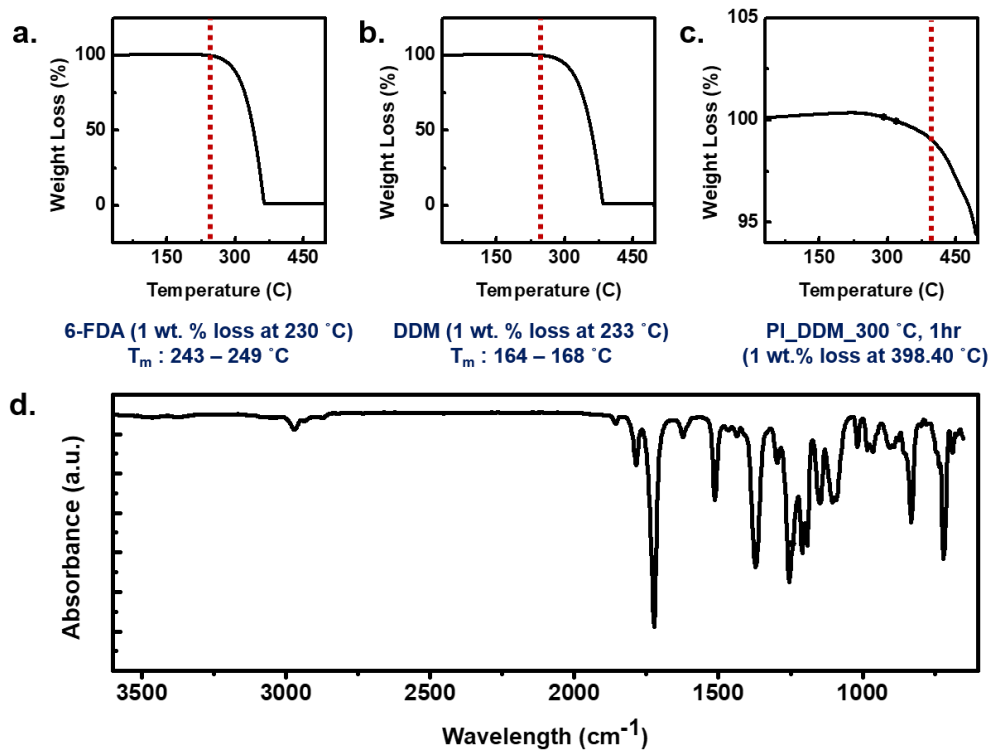
Figure 4-2. TGA data of (a) 6-FDA, (b) DDM, and (c) Polyimide. (d) FT-IR data of polyimide

4.2.2 Growth of Multilayer Graphene on a Copper Foil by Using a CVD Method

Here, multilayer graphene was synthesized on a copper foil by using a CVD method. In brief, electropolishing of copper foil with 25-μm-thick thickness (Alfa Aesar, 99.8 % purity) was applied in phosphoric acid for 15 min for surface smoothening effect. After electropolishing, the copper foil was rinsed with highly pure water followed by isopropyl alcohol treatment. Before CVD growth, electropolished copper foil was air-oxidized at 200 ˚C for 30 min on a hot plate. The copper foil was loaded into a quartz tube and located at the bottom of a quartz tube. During growth process, the temperature of CVD system was increased to 1,050 °C within 35 min with a H_2 gas flow of 200 sccm and maintained for 60 min to remove various oxides formed on a copper foil. Such process can smooth the copper surface, but also remove amorphous carbon as a form of CO. The graphene was synthesized by flowing CH_4 gas and H_2 gas (1 and 200 sccm respectively) for 120 min. After growth was over, the CVD growth was terminated under argon and vacuum condition.

4.2.3 Fabrication of Transparent Conducting Electrode of Embedded Silver Nanowires Structure with Graphene and Polyimide

AgNWs were synthesized by using a continuous flow method, and AgNW solution was prepared by dispersion of AgNWs in the mixture of IPA/distilled water at an optimized density of 0.3 mg/ml. For multilayer graphene/AgNWs/PI composite fabrication, AgNWs were spin-coated on a multilayer graphene/copper foil. Next, $AgNO_3$ dissolved in a distilled water (0.035 mM) was spin coated on the AgNW/multilayer graphene/copper foil for 60 seconds at 2000 rpm with residual time of 15 sec. After welding of AgNWs, PI dissolved in dimethylformamide (DMF, 30 wt. %) was coated on a welded-AgNWs/multilayer graphene/copper foil for direct transfer. The PI coated welded-AgNWs/multilayer graphene/copper foil was heat treated on a hot-plate at 50 ˚C for 30 min, 100 ˚C for 60 min, and 150 ˚C for 60 min for evaporation of solvent and well adhesion between welded-AgNWs/multilayer graphene/copper foil and polyimide film. Finally, copper foil was etched away by using an ammonium persulfate solution.

4.3 Figure of Merits

4.3.1 Growth Mechanism of Multilayer Graphene on a Copper Foil by Using a CVD Method

In CVD graphene growth, copper provides better control for uniformity and thickness of graphene through the self-limiting surface mechanism[83]. However, due to unavoidable various defects, single layer graphene grown by CVD methods on a copper substrate is not suitable for practical applications. CVD grown high crystalline graphene is also known to perform as an excellent barrier film for metal oxidation[84]. It is often reported that single layer graphene grown by using CVD method can prevent copper from oxidation under ambient, and high humid condition. Some reports also indicate that transferring CVD grown graphene on a metal nanowire can also efficiently prevent oxidation while maintaining its high transmittance[85]. However, due to defects present in CVD grown single layer graphene, long-term stability of barrier film property cannot be retained. For instance, CVD grown single layer graphene/copper assembly can get easily oxidized when put at 200 ˚C for 30 min[86]. The defects and copper oxide from oxidation process can be easily see by using microscope. Yet, these defects formation are impossible to avoid during CVD graphene growth process with current technology. Thus, high crystalline growth of bi- or multi-layer graphene is required to solve such problem. Recently there are reports that, introducing oxygen during CVD growth of graphene on a copper foil can result in large area of Bi- and multi-layer graphene[87]. By analyzing DFT calculation, it was reported that oxygen adsorbed on a copper foil can increase the adsorption barrier energy of carbon on a copper (i.e. Energy barrier for carbon do adsorb on pure copper (111) : 6.05 eV, oxygen pre-adsorbed copper (111) : 7.04 eV). Additionally, pre-adsorbed atomic oxygen on a copper can dramatically decrease the activation barrier of all four de-hydrogenation steps of CH_4. The pre-adsorbed oxygen on the copper surface can abstract hydrogen atom to form a hydroxyl, thereby increasing the dissociation probability. (i.e. The energy barrier for the CH_4 initial dehydrogenation on copper (111) was 1.4 eV and 3.7 (4.3) eV with the presence of oxygen and without oxygen, respectively.) It is believed that fully de-hydrogenated carbon can diffuse through bulk of copper and become ad-layer of graphene beneath the first layer of copper. Thus, it can be predicted that if copper surface is exposed to fully de-hydrogenated carbon, multilayer graphene can be grown by diffusion of carbon through bulk of copper. Here, we controlled the growth rate of a graphene by changing the location of copper foil inside a quartz tube. As it can be seen from the Figure 4-3, copper foil was either put at the center or at the bottom of a quartz tube. This can easily modify the gas precursor concentration gradient during the graphene growth since each surface will be exposed with different amount of gas. For instance, when copper foil was loaded at the center of a quartz tube, full coverage of graphene was observed at the front and back side of a copper foil (Figure 4-3b-c). However, when copper foil was put at the bottom side

of a quartz tube, only full coverage of a graphene was observed on the front side of a copper foil and partial growth of graphene was observed at the back side of a copper foil (Figure 4-3f-g). Surprisingly, single layer dominant graphene was observed for a copper foil put at the center of a quartz tube; however, multilayer graphene growth was observed when a copper foil was put at the bottom of a quartz tube (Figure 4-3d,e). Since oxidized copper was used in the experiment, we tried the same experiment, but oxidized copper foil was replaced with pure copper foil. When as-prepared copper foil was put at the center of a quartz tube, we found complete single layer graphene growth on the front side of a copper foil (Figure 4-4a). In contrast, when as-prepared copper foil was put at the bottom of a quartz tube, small multi-layer patches of graphene flakes on a single layer graphene was observed on a front side of a copper foil (Figure 4-4b). It must be noted that multi-layer graphene was only observed only when back side of a copper foil was partially grown. Thus, it can be assumed that during the growth process, decomposed carbon from methane gas could first adsorbed on the back side of a copper foil and diffused through bulk of a copper and grew as ad layers of graphene below a first layer of graphene. From Figure 4-4d, it can be noted that oxidized copper tends to show higher coverage of a multi-layer on the front side of a graphene. This also correlates to back side graphene coverage, where oxidized graphene tends to present lower coverage of graphene layer on a back side of a copper (Figure 4-4e). With such condition, we were able to enhance multi-layer graphene coverage on a front side of a copper by locating oxidized copper on the bottom of a quartz tube with increasing the reaction time. When reaction time was pro-longed to 120 min, almost fully covered multi-layer graphene was obtained at the front side of a copper foil (Figure 4-4f). To confirm the diffusion mechanism, a quartz substrate was wrapped with a copper foil and quartz wrapped copper was put at the bottom side of a quartz tube for graphene growth (Figure 4-5a). Interestingly, it was observed that complete single layer graphene was grown on the front side of a copper foil. Also, complete graphene growth on the front side of a copper foil was observed; however, no graphene growth was observed at the back side of a copper foil. It can be assumed that gas precursor was not able to penetrate inside a quartz wrapped copper foil, thereby, no graphene was grown at the back side of a copper foil (Figure 4-5b-d).
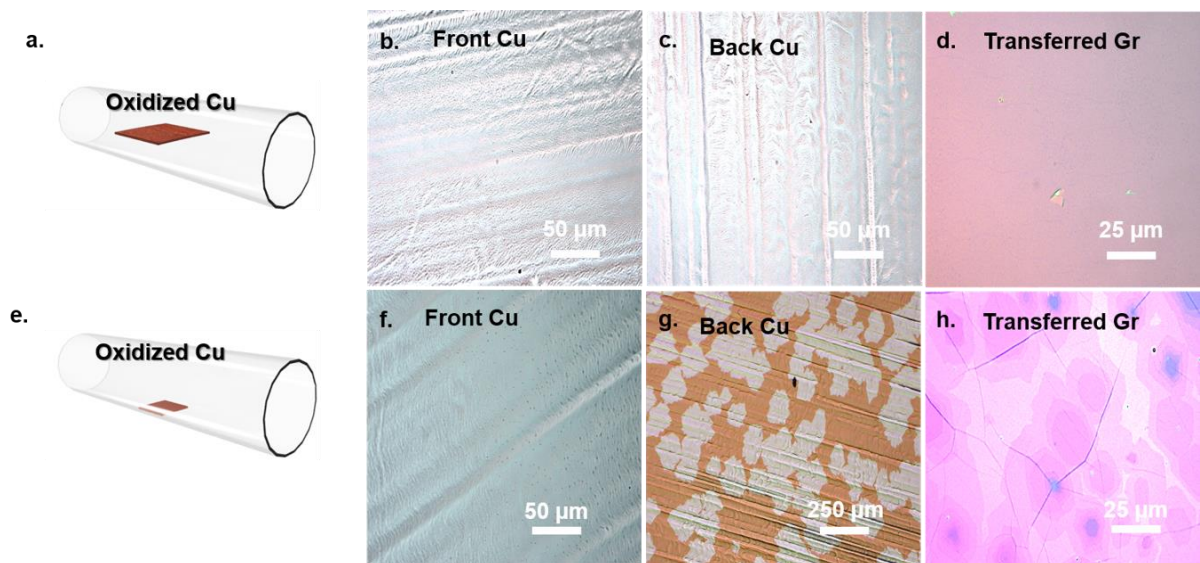
Figure 4-3. (a,e) Schematics of copper foil loading location during CVD graphene growth inside a quartz tube. (b,c) Optical images of graphene/copper foil after oxidation at 200 ˚C for 30 min. (d) An optical image of transferred CVD grown graphene from the front surface of copper foil. (f-g) Optical images of graphene/copper foil after oxidation at 200 ˚C for 30 min. (h) An optical image of transferred CVD grown graphene from the front surface of copper foil.
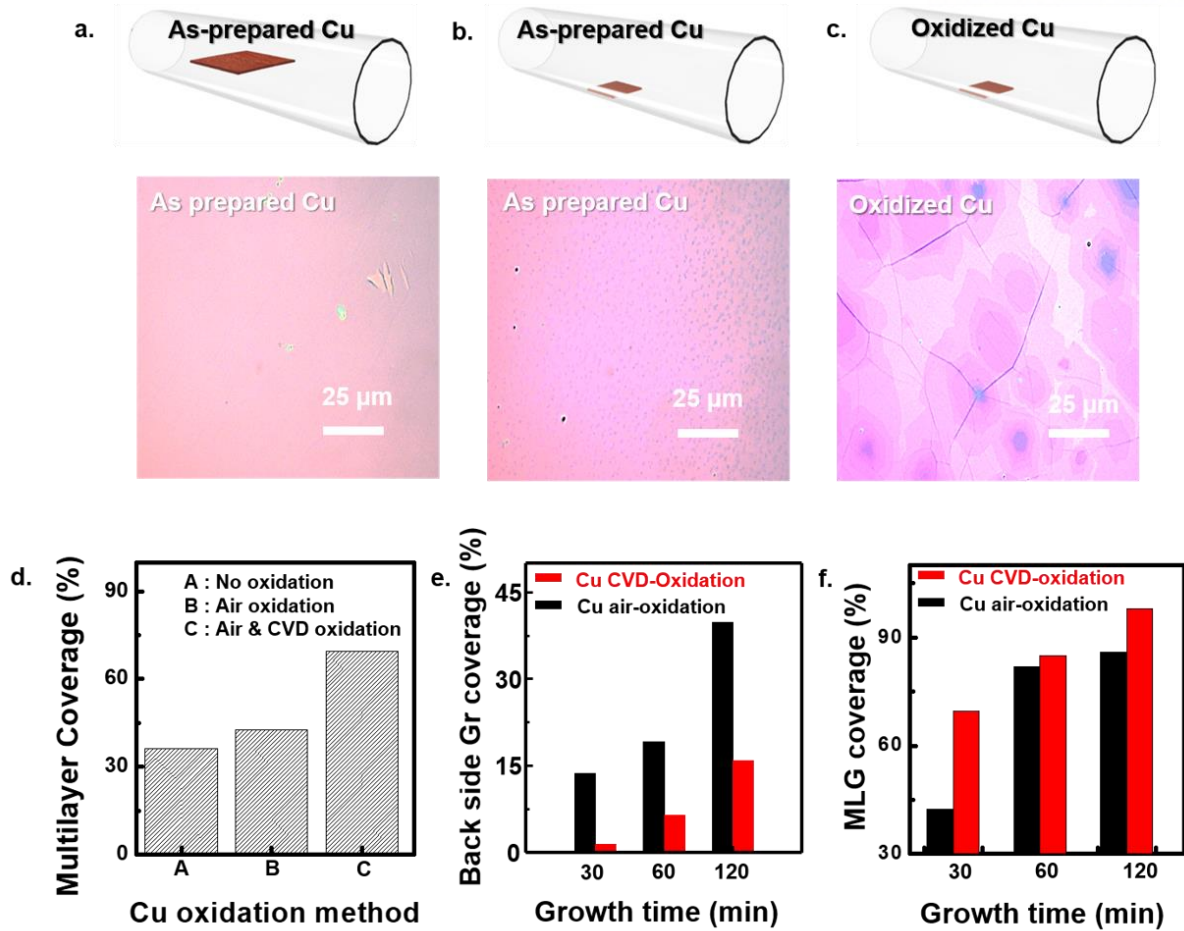
Figure 4-4. (a-c) Schematics of copper foil treatment and loading location during CVD graphene growth. Mono layer graphene growth was only observed when copper foil was located at the center of a quartz tube; however, large number of small multi-layer flake was observed when copper foil was located at the bottom of a quartz tube. Additionally, size of multilayer graphene flakes increased when a copper foil was oxidized. (d) Dependence of multilayer graphene coverage data by copper oxidation method. (e) Relationship between back side graphene coverage and copper foil oxidation method after graphene growth. (f) Relationship between multilayer graphene coverage data with growth time.

Figure 4-5. (a) Photo and schematic images of Al_2O_3 substrate wrapped by a copper foil. (b-c) Optical microscope images of graphene/copper foil after 200 ˚C annealing treatment. (d) An optical microscope image of graphene transferred on a Si/SiO$_2$ substrate.

4.3.2 Embedded Silver Nanowires Structure with Graphene and Polyimide

Various graphene/AgNW composite film has been reported by numerous research groups. In most of the cases, graphene is used as a barrier film to protect AgNWs from degradation under ambient conditions such as oxidation and sulfurization. Typically, graphene/AgNW composite film is fabricated by first coating AgNW networks on a substrate, and second wet-transfer of a graphene layer on spin-coated AgNW networks substrate. Graphene oxide is also widely used for graphene/AgNW composite film for its facile method. However, these methods have some draw backs. Wet transfer of CVD grown graphene from a copper foil to AgNW substrate can lead tears of graphene during transfer process due to rough surface of AgNWs. Graphene oxide contain lots of defects and it's not suitable for long-term barrier film. Unlike other reports, multilayer graphene/AgNW/PI composite film fabrication process was done on the multilayer graphene grown copper foil. It was very important to use multilayer grown graphene copper foil because, during copper foil etching process step, copper etchant solution can get contact with AgNWs through graphene defects since AgNWs are coated right above graphene layers. Figure 4-6a Illustrates schematics of multilayer graphene/AgNW/PI composite film fabrication process. First, multi-layer graphene was grown on a copper foil by using a CVD method. AgNWs were then spin-coated on a copper foil. By controlling the coating number on a MLG/Cu foil, density of AgNWs were well controlled. Next, AgNWs were welded by using chemical welding method. When welding process is over, transparent polyimide solution was coated on a welded-AgNW/multilayer graphene/copper foil for direct transfer. The PI coated welded-AgNW/multilayer graphene/copper was heat treated on a hot-plate at 50 °C for 30 min, 100 °C for 60 min, and 150 °C for 60 min for evaporation of solvent and well adhesion between welded-AgNW/multilayer graphene/copper foil and polyimide film. Finally, copper foil was etched away by using an ammonium persulfate solution. The welded-AgNW/multilayer graphene/PI composite film was transparent as shown if Figure 4-6b. Interestingly, embedded welded-AgNWs were observed by using SEM (Figure 4-6c-e). The embedded structure of AgNWs were well buried under multilayer graphene and tears and wrinkle of multilayer graphene crossing over AgNWs were observed. The multilayer graphene was analyzed by using Raman spectroscopy. High crystalline multilayer graphene was confirmed, and by analyzing random 100 spot, 44 % of the multilayer graphene was AB-stacked where 56 % of the multi-layer graphene was randomly oriented (Figure 4-6f).
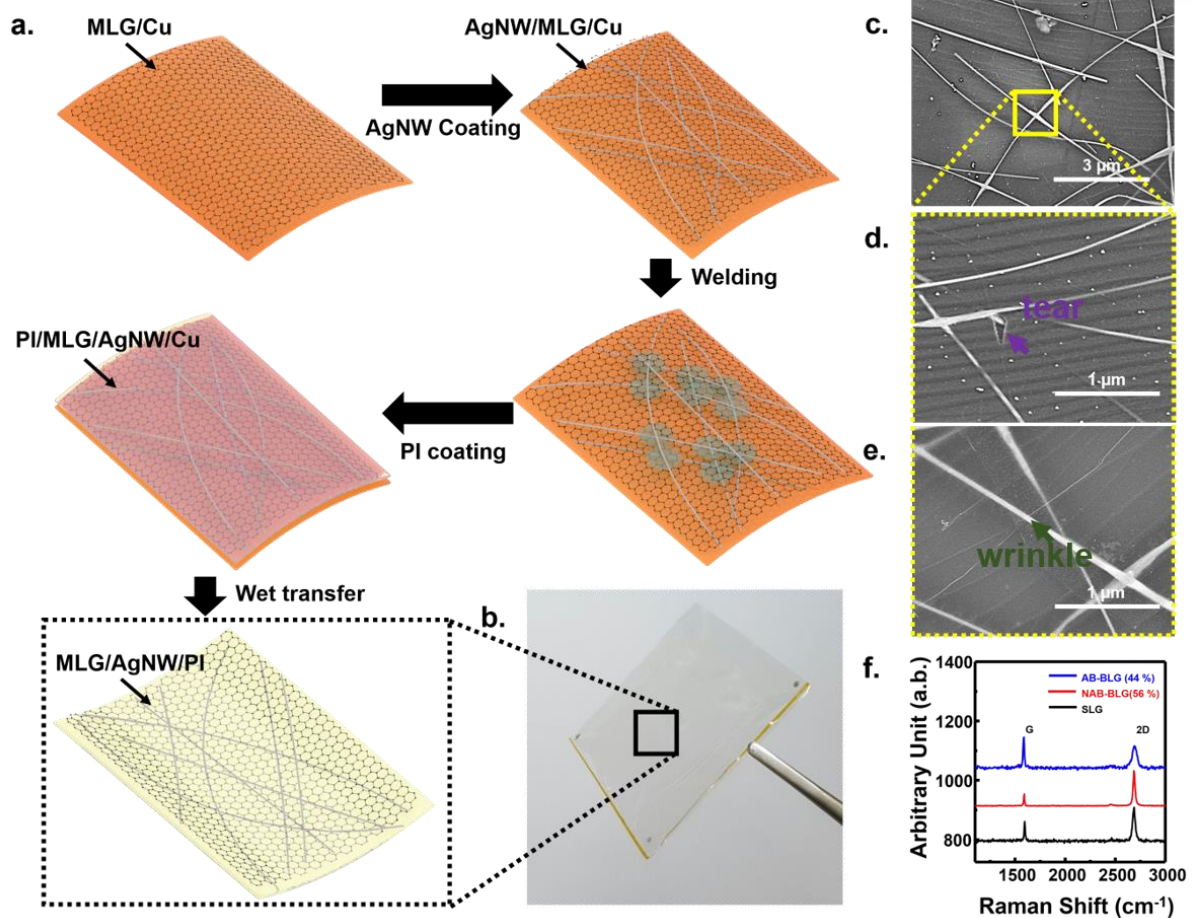
Figure 4-6. (a) A schematic illustration of MLG/AgNW/PI fabrication method. (b) a photo image of the composite film held by tweezer. (c-d) SEM images of MLG/AgNW/PI composite film. A purple and green arrow indicate graphene tear and wrinkle. (f) Raman spectrum of MLG grown on a Cu foil

4.3.3 Opto-electronic Property of Multilayer Graphene and Multilayer Graphene/Silver Nanowires/Polyimide Composite

As shown in Figure 4-7, opto-electronic property of CVD grown graphene and multilayer graphene/AgNW/PI composite was analyzed by using van der paw methods through hall measurement apparatus. Figure 4-7a show sheet resistance and transmission data of CVD grown graphene with respect to multilayer graphene coverage portion. Single layer dominant graphene exhibited 750 ± 30 ohm/sq at 97.3 ± 0.3 % of transmittance at visible ranges. As multilayer graphene portion on a single layer graphene increased from 42, 70, and 98 %, the sheet resistance and transmittance at visible ranges also changed from 330 ± 41, 280 ± 47, and 246 ± 31 ohm/sq with 96.8 ± 1, 95.9 ± 1.1, and 95.4 ± 1.3 % respectively. Since scope of this experiment is to use graphene with high coverage of multilayer graphene, AgNWs were spin coated on a graphene with 98 % coverage of multilayer graphene. By changing the number of spin-coating of AgNWs from 1 to 4 times on a multilayer graphene layers,

sheet resistance and transmission at visible ranges were changed from 125 ± 17, 67 ± 13, 43 ± 13, and 24 ± 5 ohm/sq with 93.1 ± 1.4, 91 ± 1.1, 88.7 ± 1.3, and 85.4 ± 1.2 % respectively (Figure 4-7b). It is well reported that opto-electronic properties of AgNWs largely depend on contact between each nanowires. In most of the cases, insulating polymer residue is adhered on the walls of AgNWs. Such insulating polymer can increase the contact resistance between each AgNWs. Thus, it is important to improve metal contact. In this experiment, chemical welding of AgNWs were applied to improve the contact between each AgNWs. In brief, 0.035 mM of $AgNO_3$ solution was prepared and spin coated on an AgNW/multilayer graphene/copper foil at 2000 rpm for 60 seconds with a residual time of 15 sec. Due to galvanic displacement reaction from Ag^+ and exposed copper foil, electrons were transferred to an Ag^+ and reduced Ag^0 were transferred to AgNW junction where high electrostatic force exist. By repeating such methods up to 4 times, almost all AgNWs on a multilayer graphene/copper foil was welded. Figure 4-7c shows such welding process were very effective and reduced sheet resistance significantly. When 5 times of welding process was applied on different number of AgNWs coated multilayer graphene from 1 to 4 times, 69.6 %, 50.7 %, 44.1 %, and 42 % of sheet resistance reduction were observed. This was attributed to excellent welding process by simple supplement of Ag^o on the junction of AgNWs by using galvanic displacement. Finally, it can be noted that our fabricated multilayer graphene/AgNW/PI composite film is well suited for TCEs when compared to other opto-electronic performance of TCEs (Figure 4-7d).
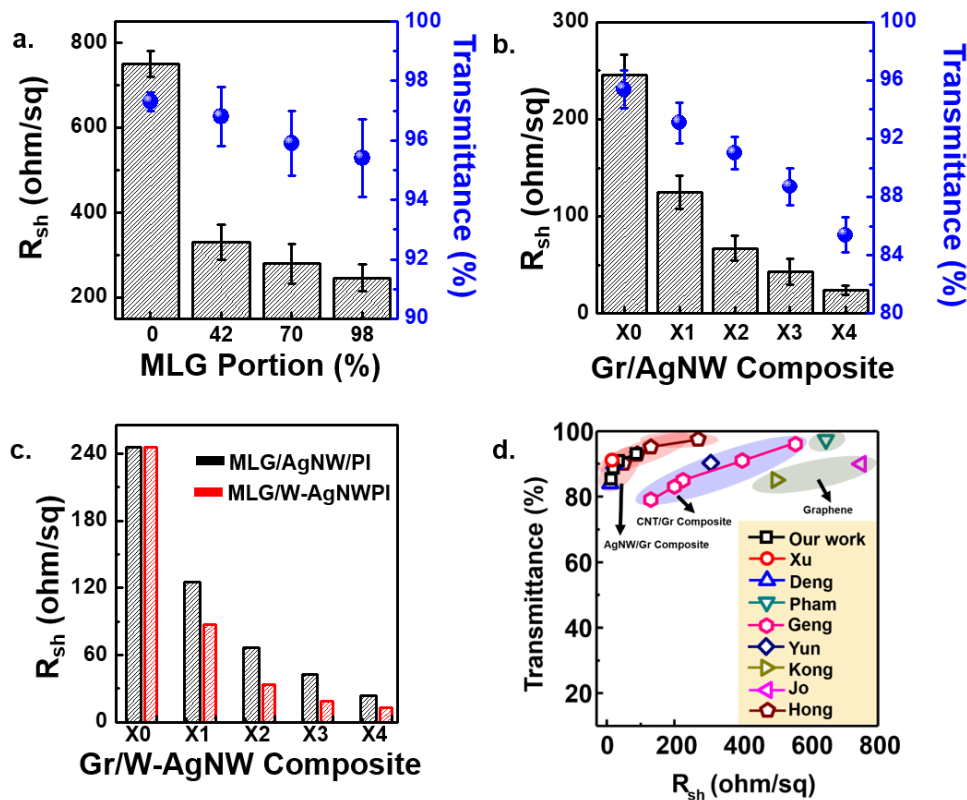
Figure 4-7. (a) An opto-electrical data of a Gr/PI composite film. Both transmission and sheet resistance value decreased as multilayer graphene portion on a single layer graphene increased. (b) An opto-electrical data of a multilayer graphene/AgNW/PI. When spin-coating number of AgNW increased, reduction of sheet resistance and transmittance were observed. (c) Effect of sheet resistance reduction after welding of AgNWs on a multilayer graphene/AgNW/PI composite. (d) Transmission and sheet resistance data comparison with other transparent conducting electrodes.

4.3.4 Mechanical Properties of Silver Nanowires/Polyimide, Multilayer Graphene/Polyimide and Multilayer Graphene/Silver Nanowires/Polyimide Composite

Here, we have tested mechanical stability under bending of multilayer graphene, AgNWs, and multilayer graphene/AgNW/PI composite. As it can be seen from the Figure 4-8a, as bending cycle was increased for each TCEs, highest resistance increase was observed for AgNW/PI composite film. Multilayer graphene, and multilayer graphene/AgNW/PI composite film showed most stable under bending cycles up to 1,000 times. Figure 4-8b shows resistance change upon bending of each films under various bending radius. Unlike multilayer graphene/AgNW/PI composite film, multilayer graphene/PI and AgNW/PI composite film's resistance sharply increased when bending was performed with bending radius < 20 mm. However, multilayer graphene/AgNW/PI showed very stable under bending. Only little change of resistance under bending with bending radius <10 mm was observed. We

believe that partially embedded structure of AgNWs under polyimide and graphene strongly acted as concrete and retained its original structure during bending.
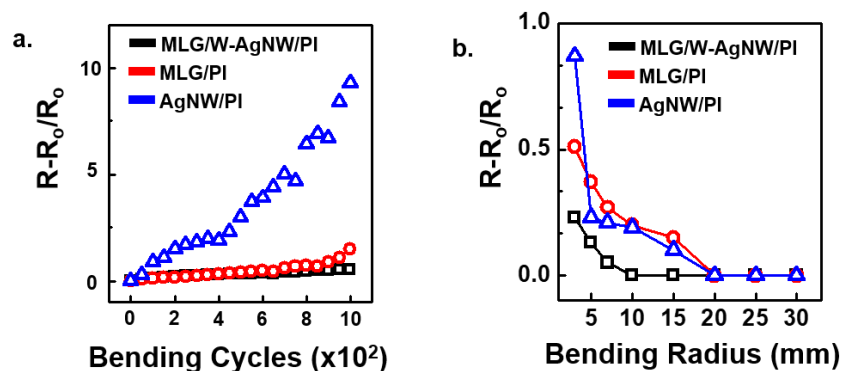
Figure 4-8. Mechanical properties of multilayer graphene/AgNW/PI composite film. (a) bending cycle, and (b) bending radius.

4.3.5 Environmental Stability Study of Silver Nanowires/Polyimide, Multilayer Graphene/Polyimide, and Multilayer Graphene/Silver Nanowires/Polyimide Composite

TCEs fabricated by incorporating AgNWs show weak at long-term stability which closely correlates to the degradation of AgNWs under ambient conditions. It is widely known that silver nanomaterials easily get oxidized or sulfurized under ambient conditions due to large specific surface area. For example, such degradations are highly related to their size, chemical composition, and surface structure of silver nanoparticles which often extremely changes even after couple of days due to the reactions under ambient condition. Since AgNWs, which grow from multiply twinned particles with defects and dislocations, are more sensitive in oxidation and sulfurization. These ambient conditions include high temperature, high humidity, light irradiation, or even at room temperature. Due to such undesired degradation of AgNWs, their structure severely changes and become disconnected after couple of days. These degradations can cause shorts in conducting channels and increase contact resistance between each AgNWs. Therefore, it is necessary to protect surface exposed TCEs consists of AgNWs, and prevent the conditions that can harm AgNWs from oxidation or sulfurization. Here, long-term environmental study was analyzed by testing the resistance change of multilayer graphene/AgNW/PI, multilayer graphene/PI, and AgNW/PI composite films under ambient condition, 100 ˚C, and sulfurization. First, the composite films were left at room temperature for 60 days (Figure 4-9a). Multilayer graphene/PI and multilayer graphene/AgNW/PI film showed very stable without any noticeable changes of resistance under ambient condition for 60 days; however, AgNW/PI composite film showed large changes of resistance as time elapsed. Similarly, composite films were tested at 100 ˚C for 10 days, and only sharp increase of resistance changes were observed for AgNW/PI composite

film. In contrast, multilayer graphene/AgNW/PI composite film and multilayer graphene/PI composite film were stable under 100 ˚C for 10 days (Figure 4-9b). It is known highly crystalline CVD grown graphene is inert and stable under ambient condition and at high temperature. In addition, high crystalline structure of multilayer graphene layers compensates each other to overcome structural defects and acted as perfect barrier film for AgNWs to prevent from oxidation. Sulfurization test was performed and demonstrated at Figure 4-9c. When AgNWs/PI composite film was treated with ammonium persulfate solution, immediately resistance changes were observed and shorted at 7 min. However, multilayer graphene/PI and multilayer graphene/AgNW/PI composite film stayed stable up to 7 hours of treatment.
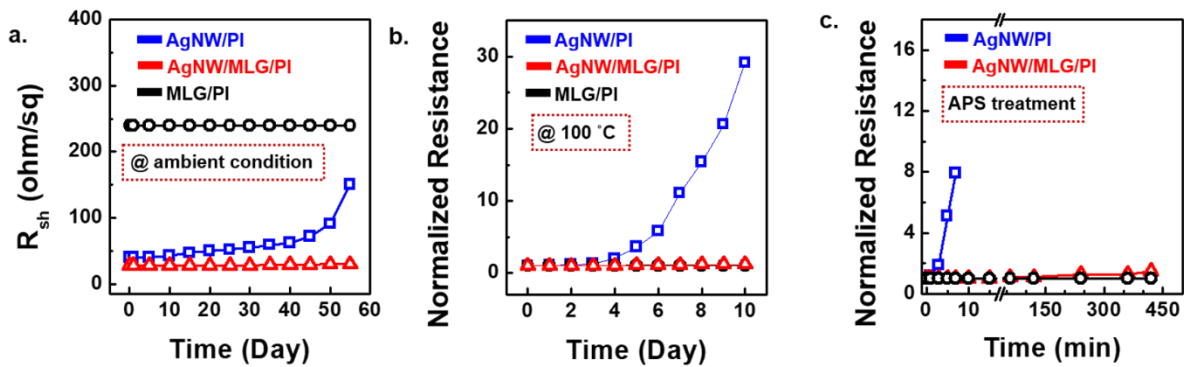
Figure 4-9. Environmental test of multilayer graphene/AgNW/PI at (a) 100 ˚C under ambient condition, (b) room temperature under ambient condition, and (c) sulfurization by immersing the composite film in ammonium persulfate solution

4.4 Conclusion

Highly performance with long-term stability of multilayer graphene/AgNW/PI composite TCEs were fabricated on a copper foil. By studying the multilayer graphene growth mechanism, nearly full coverage of multilayer graphene was grown on a copper foil and served as an excellent barrier film for silver nanowire networks. We have determined that high crystalline multilayer graphene could effectively act as a barrier film under various conditions. The high flexibility and mechanical property of multilayer graphene/AgNW/PI composite is due to partially embedded structure of AgNWs under transparent polyimide and multilayer graphene layers. We believe that such TCEs can be further improved by adjusting the layer uniformity of graphene on a copper foil by optimizing the growth parameters.

Conclusion

The electrification on various industry fields are requiring high technology. In display technology, which is one of the most closely related to us in daily bases, TCEs for next generation application should possess excellent properties in flexibility, bendability, and stretchability. In addition, TCEs containing devices must operate at harsh environment that can provide long-term stability. Yet, current alternative conducting materials cannot seldomly used to satisfy all the requirements stated above. In this thesis, various conducting materials including carbon nanotubes (CNTs), graphene and silver nanowires (AgNWs) were studied and demonstrated as a transparent conducting electrode (TCE) for practical applications. Since chemical vapor deposition (CVD) grown graphene with current technology always exhibit unavoidable defects, uniform coating of highly conducting single-walled carbon nanotubes (SWCNTs) on a graphene layer was suggested and enhancement of overall performance was observed. Although optoelectronic and mechanical properties with thermal stability of doped SWCNT/graphene composite showed enhanced performance, the electrical properties with transmittance at visible ranges was not enough for practical applications. To meet the industry criteria, AgNWs based TCEs were demonstrated and novel synthesis methods was developed for uniform and stable synthesis of AgNWs. In addition, multilayer graphene with high thermal stable transparent polyimide polymer film was introduced as a barrier film to prevent AgNWs oxidation. With high crystalline multilayer graphene, the long-term stability issue of AgNWs based TCEs were settled and unique structure of partially embedded AgNWs showed excellent opto-electrical, mechanical properties which performed better than other TCEs reported. Although such TCEs film was fabricated by using expensive equipment and process, I believe that proposed process engineering and design of unique structure will contribute the potentiality for high performance TCEs for practical applications. I also believe that continuous research and study will find a solution and alternatively replace ITO in the future for various practical applications.

References

1. Mazur, M.; Doraradzki. J.; Kaczmarek. D.; Moh. S.' Placido. F., Sheet resistance and optical properties of ITO thin films deposited by magnetron sputtering with different O_2/Ar flow ratio. 2010 International Students and Young Scientists Workshop,, Photonics and Microsystems" 2010, 60-63

2. Tvingstedt, K.; Inganäs, O., Electrode Grids for ITO Free Organic Photovoltaic Devices. Advanced Materials 2007, 19, 2893-2897.

3. Alzoubi, K.; Hamasha, M. M.; Lu, S.; Sammakia, B., Bending Fatigue Study of Sputtered ITO on Flexible Substrate. Journal of Display Technology 2011, 7, 593-600.

4. Hsu, P. C.; Wang, S.; Wu, H.; Narasimhan, V. K.; Kong, D.; Ryoung Lee, H.; Cui, Y., Performance enhancement of metal nanowire transparent conducting electrodes by mesoscale metal wires. Nat Commun 2013, 4, 2522.

5. Snook, G. A.; Kao, P.; Best, A. S., Conducting-polymer-based supercapacitor devices and electrodes. Journal of Power Sources 2011, 196, 1-12.

6. Lin, K.; Kumar, R. S.; Cheng, L. S.; Jin, C. S., Performance Improvement of Carbon-Nanotube-Incorporated Transparent Conducting Anode Film for Organic Device Application. IEEE Transactions on Electron Devices 2009, 56, 31-37.

7. Cheon, Y.; Nam, J.; Kim, C. S.; Jo, S., Reduced yellowing of silver nanowire transparent conductive electrodes by simple hydrazine treatment. AIP Advances 2017, 7, 025215.

8. Padmalekha, K. G.; Admassie, S., Electrochromic, magnetotransport and AC transport properties of vapor phase polymerized PEDOT (VPP PEDOT). Synthetic Metals 2009, 159, 1885-1889.

9. Yan, J.; Sun, C.; Tan, F.; Hu, X.; Chen, P.; Qu, S.; Zhou, S.; Xu, J., Electropolymerized poly(3,4-ethylenedioxythiophene):poly(styrene sulfonate) (PEDOT:PSS) film on ITO glass and its application in photovoltaic device. Solar Energy Materials and Solar Cells 2010, 94, 390-394.

10. Wang, J.; Cai, G.; Zhu, X.; Zhou, X., Oxidative chemical polymerization of 3, 4-ethylenedioxythiophene and its applications in antistatic coatings. Journal of Applied Polymer Science 2012, 124, 109-115.

11. Ouyang, J., "Secondary doping" methods to significantly enhance the conductivity of PEDOT:PSS for its application as transparent electrode of optoelectronic devices. Displays 2013, 34, 423-436.

12. Xing, Y.; Qian, M.; Wang, G.; Zhang, G.; Guo, D.; Wu, J., UV irradiation induced conductivity improvement in poly(3,4-ethylenedioxythiophene):poly(styrenesulfonate) film. Science China Technological Sciences 2013, 57, 44-48.

13. Lee. S. M.; Kim. J. H.; Ahn. J. H., Graphene as a flexible electronic material: mechanical limitations by defect formation and efforts to overcome. Mater. Today., 2015, 18, 336-344

14. McKitterick, C. B.; Prober, D. E.; Rooks, M. J., Electron-phonon cooling in large monolayer graphene devices. Physical Review B 2016, 93.

15. Banszerus. L.; Schmitz. M.; Engels. S.; Dauber. J.; Oellers. M.; Haupt. F.; Watanabe. K.; Taniguchi. T.; Beschoten. B.; Stampfer. C., Ultrahigh-mobility graphene devices from chemical vapor deposition on reusable copper. Sci. Adv., 2015, 1500222-

16. Liu, C. H.; Chen, Q.; Liu, C. H.; Zhong, Z., Graphene Ambipolar Nanoelectronics for High Noise Rejection Amplification. Nano Lett 2016, 16, 1064-8.

17. Lafont, F.; Ribeiro-Palau, R.; Kazazis, D.; Michon, A.; Couturaud, O.; Consejo, C.; Chassagne, T.; Zielinski, M.; Portail, M.; Jouault, B.; Schopfer, F.; Poirier, W., Quantum Hall resistance standards from graphene grown by chemical vapour deposition on silicon carbide. Nat Commun 2015, 6, 6806.

18. McKitterick, C. B.; Prober, D. E.; Rooks, M. J., Electron-phonon cooling in large monolayer graphene devices. Physical Review B 2016, 93.

19. Zhang, Y.; Zhang, H.; Li, F.; Shu, H.; Chen, Z.; Sui, Y.; Zhang, Y.; Ge, X.; Yu, G.; Jin, Z.; Liu, X., Invisible growth of microstructural defects in graphene chemical vapor deposition on copper foil. Carbon 2016, 96, 237-242.

20. Kuruvilla, N.; Raina, J. P., Impact of Bundle Structure on Performance of on-Chip CNT Interconnects. Journal of Nanotechnology 2014, 2014, 1-8.

21. Fernandes, R. M.; Abreu, B.; Claro, B.; Buzaglo, M.; Regev, O.; Furo, I.; Marques, E. F., Dispersing Carbon Nanotubes with Ionic Surfactants under Controlled Conditions: Comparisons and Insight. Langmuir 2015, 31, 10955-65.

22. Li, F.; Tang, B.; Xiu, J.; Zhang, S., Hydrophilic Modification of Multi-Walled Carbon Nanotube for Building Photonic Crystals with Enhanced Color Visibility and Mechanical Strength. Molecules 2016, 21.

23. Di Crescenzo, A.; Ettorre, V.; Fontana, A., Non-covalent and reversible functionalization of carbon nanotubes. Beilstein J Nanotechnol 2014, 5, 1675-90.

24. Reddy, K. R.; Sin, B. C.; Yoo, C. H.; Sohn, D.; Lee, Y., Coating of multiwalled carbon nanotubes with polymer nanospheres through microemulsion polymerization. J Colloid Interface Sci 2009, 340, 160-5.

25. Song, Y. I.; Kim, G. Y.; Choi, H. K.; Jeong, H. J.; Kim, K. K.; Yang, C. M.; Lim, S. C.; An, K. H.; Jung, K. T.; Lee, Y. H., Fabrication of Carbon Nanotube Field Emitters Using a Dip-Coating Method. Chemical Vapor Deposition 2006, 12, 375-379.

26. Abe, S.; Nakayam, K.; Hayashi, D.; Akasaka, T.; Uo, M.; Watari, F.; Takada, T., Development of a novel transparent substrate coated by carbon nanotubes through covalent bonding. Physics

Procedia 2011, 14, 147-151.

27. Holubowitch, N. E.; Landon, J.; Lippert, C. A.; Craddock, J. D.; Weisenberger, M. C.; Liu, K., Spray-Coated Multiwalled Carbon Nanotube Composite Electrodes for Thermal Energy Scavenging Electrochemical Cells. ACS Appl Mater Interfaces 2016, 8, 22159-67.

28. Omi, F. R.; Choudhury, M. R.; Anwar, N.; Bakr, A. R.; Rahaman, M. S., Highly Conductive Ultrafiltration Membrane via Vacuum Filtration Assisted Layer-by-Layer Deposition of Functionalized Carbon Nanotubes. Industrial & Engineering Chemistry Research 2017, 56, 8474-8484.

29. Moon, J. S.; Park, J. H.; Lee, T. Y.; Kim, Y. W.; Yoo, J. B.; Park, C. Y.; Kim, J. M.; Jin, K. W., Transparent conductive film based on carbon nanotubes and PEDOT composites. Diamond and Related Materials 2005, 14, 1882-1887.

30. Beecher, P.; Servati, P.; Rozhin, A.; Colli, A.; Scardaci, V.; Pisana, S.; Hasan, T.; Flewitt, A. J.; Robertson, J.; Hsieh, G. W.; Li, F. M.; Nathan, A.; Ferrari, A. C.; Milne, W. I., Ink-jet printing of carbon nanotube thin film transistors. Journal of Applied Physics 2007, 102, 043710.

31. Lee. S. W.; Kim. B. S.; Chen. S.; Yang. S. H.; Hammond. P. T.; Layer-by-Layer Assembly of All Carbon Nanotube Ultrathin Films for Electrochemical Applications. J. Am. Chem. Soc. 2009, 131, 671-679

32. Bardecker. J. A.; Afzali. A.; Tulevski. G. S.; Graham. T.; Hannon. J. B.; Jen. A. K. Y., Directed Assembly of Single-Walled Carbon Nanotubes via Drop-casting onto a UV-Patterned Photosensitive Monolayer. J. Am. Chem. Soc., 2008, 130, 7226-7227

33. Ago. H.; Ito. Y.; Mizuta. N.; Yoshida. K.; Hu. B.; Orofeo. C. M.; Tsuji. M.; Ikeda. K.; Mizuno. S., Epitaxial chemical vapor deposition growth of single-layer graphene over cobalt film crystallized on sapphire. ACS NANO., 2010, 4, 7407

34. Kim. K. S.; Zhao. Y.; Jang. H.; Lee. S. Y.; Kim. J. M.; Kim. K. S.; Ahn. J. H.; Kim. P.; Choi. J. Y.; Hong. B. H., Nature., 2009, 457, 706

35. Loginova. E.; Bartelt. N. C.; Feibelman. P. J.; McCarty. K. F., New. J. Phys., 2009, 11, 063046

36. Gao. L.; Ren. W.; Xu. H.; Jin. L.; Wang. Z.; Ma. T.; Zhiyong. L. P.; Fu. Q.; Peng. L. M.; Bao. X.; Cheng. H. M., Nat. Commun., 2012, 3, 699

37. Li. X.; Cai. W.; An. J.; Kim. S.; Nah. J.; Yang. D.; Piner. R.; Velamakanni. A.; Jung. I.; Tutuc. E.; Banerjee. S. K.; Colombo. L.; Ruoff. R. S., Science., 2009, 324, 1312

38. Kalbac. M.; Frank. O.; Kavan. L., Carbon., 2012, 50, 3682

39. Long, F.; Yasaei, P.; Yao, W.; Salehi-Khojin, A.; Shahbazian-Yassar, R., Anisotropic Friction of Wrinkled Graphene Grown by Chemical Vapor Deposition. ACS Appl Mater Interfaces 2017, 9, 20922-20927.

40. Suk. J. W.; Kitt. A.; Magnuson. C. W.; Hao. Y.; Ahmed. S.; An. J.; Swan. A. K.; Goldberg. B.

B.; Ruoff. R. S., Transfer of CVD-Grown Monolayer Graphene onto Arbitrary Sybstrates. ACS NANO 2011, 5, 6916-6924

41. Tsen. A. W.; Brown. L.; Levendorf. M. P.; Ghahari. F.; Huang. P. Y.; Havener. R. W.; Ruiz-Vargas. C. S.; Muller. D. A.; Kim. P.; Park. J., Tailoring electrical transport across grain boundaries in polycrystalline graphene. Science., 2012, 336, 1143

42. Wang. H.; Wang. G.; Bao. P.; Yang. S.; Zhu. W.; Xie. X.; Zhang. W. J., Controllable synthesis of submillimeter single-crystal monolayer graphene domains on copper foils by suppressing nucleation. JACS., 2012, 134, 3627-3630

43. Nguyen. V. L.; Shin. B. G.; Duong. D. L.; Kim. S. T.; Perello. D.; Lim. Y. J.; Yuan. Q. H.; Ding. F.; Jeong. H. Y.; Shin. H. S.; Lee. S. M.; Chae. S. H.; Vu. Q. A.; Lee. S. H.; Lee. Y. H., Seamless Stitching of graphene domains on polished copper (111) foil. Adv. Mater., 2015, 27, 1376-1382

44. Tung. V. C.; Chen. L. M.; Allen. M. J.; Wassei. J. K.; Nelson. K.; Kaner. R. B.; Yang. Y.; Low-temperature solution processing of graphene-carbon nanotube hybrid materials for high-performance transparent conductors. Nano. Lett., 2009, 9, 1949-1955

45. Dong. X.; Li. B.; Wei. A.; Cao. X.; Chan-Park. M. B.; Zhang. H.; Li. L. J.; Huang. W.; Chen. P., One-step growth of graphene-carbon nanotube hybrid materials by chemical vapor deposition. Carbon., 2011, 49, 2944-2949

46. Yu. D.; Dai. L., Self-assembled graphene/carbon nanotube hybrid films for supercapacitors. J. Phys. Chem. Lett., 2009, 1, 467-470

47. Kim. S. H.; Song. W.; Jung. M. W.; Kang. M. A.; Kim. K.; Chang. S. J.; Lee. S. S.; Lim. J.; Hwang. J.; Myung. S.; An. K. S., Carbon nanotube and graphene hybrid thin film for transparent electrodes and field effect transistors. Adv. Mater., 2014, 26, 4247-4252

48. Kasry. A.; Kuroda. M. A.; Martyna. G. J.; Tulevski. G. S.; Bol. A. A., Chemical Doping of Large-Area Stacked Graphene Films for Use as Transparent Conducting Electrodes. ACS NANO 2010, 4, 3839-3844

49. Shi, S. F.; Tang, T. T.; Zeng, B.; Ju, L.; Zhou, Q.; Zettl, A.; Wang, F., Controlling graphene ultrafast hot carrier response from metal-like to semiconductor-like by electrostatic gating. Nano Lett 2014, 14, 1578-82.

50. Cusati, T.; Fiori, G.; Gahoi, A.; Passi, V.; Lemme, M. C.; Fortunelli, A.; Iannaccone, G., Electrical properties of graphene-metal contacts. Sci Rep 2017, 7, 5109.

51. Li. X.; Wang. H.; Robinson. J. T.; Sanchez. H.; Diankov. G.; Dai. H., Simultaneous Nitrogen Doping and Reduction of Graphene Oxide. J. Am. Chem. Soc 2009, 131, 15939-15944

52. Jafari, A.; Ghoranneviss, M.; Salar Elahi, A., Growth and characterization of boron doped graphene by Hot Filament Chemical Vapor Deposition Technique (HFCVD). Journal of Crystal Growth 2016, 438, 70-75.

53. D'Arsié, L.; Esconjauregui, S.; Weatherup, R. S.; Wu, X.; Arter, W. E.; Sugime, H.; Cepek, C.; Robertson, J., Stable, efficient p-type doping of graphene by nitric acid. RSC Advances 2016, 6, 113185-113192.

54. Bari, B.; Lee, J.; Jang, T.; Won, P.; Ko, S. H.; Alamgir, K.; Arshad, M.; Guo, L. J., Simple hydrothermal synthesis of very-long and thin silver nanowires and their application in high quality transparent electrodes. Journal of Materials Chemistry A 2016, 4, 11365-11371.

55. Hsieh, C.-T.; Tzou, D.-Y.; Pan, C.; Chen, W.-Y., Microwave-assisted deposition, scalable coating, and wetting behavior of silver nanowire layers. Surface and Coatings Technology 2012, 207, 11-18.

56. Han, C. J.; Park, B.-G.; Suk Oh, M.; Jung, S.-B.; Kim, J.-W., Photo-induced fabrication of Ag nanowire circuitry for invisible, ultrathin, conformable pressure sensors. Journal of Materials Chemistry C 2017, 5, 9986-9994.

57. Lee, E.-J.; Chang, M.-H.; Kim, Y.-S.; Kim, J.-Y., High-pressure polyol synthesis of ultrathin silver nanowires: Electrical and optical properties. APL Materials 2013, 1, 042118.

58. Deignan, G.; Goldthorpe, I. A., The dependence of silver nanowire stability on network composition and processing parameters. RSC Advances 2017, 7, 35590-35597.

59. Abalde-Cela, S.; Taladriz-Blanco, P.; de Oliveira, M. G.; Abell, C., Droplet microfluidics for the highly controlled synthesis of branched gold nanoparticles. Sci Rep 2018, 8, 2440.

60. Gottesman, R.; Tangy, A.; Oussadon, I.; Zitoun, D., Silver nanowires and nanoparticles from a millifluidic reactor: application to metal assisted silicon etching. New Journal of Chemistry 2012, 36, 2456.

61. Chou, K.-S.; Hsu, C.-Y.; Liu, B.-T., Salt-mediated polyol synthesis of silver nanowires in a continuous-flow tubular reactor. RSC Advances 2015, 5, 29872-29877.

62. Ren, M.; Jin, Y.; Chen, W.; Huang, W., Rich Capping Ligand–Ag Colloid Interactions. The Journal of Physical Chemistry C 2015, 119, 27588-27593.

63. Ran, Y.; He, W.; Wang, K.; Ji, S.; Ye, C., A one-step route to Ag nanowires with a diameter below 40 nm and an aspect ratio above 1000. Chem Commun (Camb) 2014, 50, 14877-80.

64. Wiley, B.; Sun, Y.; Mayers, B.; Xia, Y., Shape-controlled synthesis of metal nanostructures: the case of silver. Chemistry 2005, 11, 454-63.

65. Coskun, S.; Aksoy, B.; Unalan, H. E., Polyol Synthesis of Silver Nanowires: An Extensive Parametric Study. Crystal Growth & Design 2011, 11, 4963-4969.

66. Jiu, J.; Suganuma, K., Metallic Nanowires and Their Application. IEEE Transactions on Components, Packaging and Manufacturing Technology 2016, 6, 1733-1751.

67. Reina. A.; Jia. X.; Ho. J.; Nezich. D.; Son. H.; Bulvic. V.; Dresselhaus. M. S.; Kong. J., Large Area, Few-Layer Graphene Films on Arbitrary Substrates by Chemical Vapor Deposition. Nano Lett 2009, 9, 30-35

68. Kim, K. S.; Zhao, Y.; Jang, H.; Lee, S. Y.; Kim, J. M.; Kim, K. S.; Ahn, J. H.; Kim, P.; Choi, J. Y.; Hong, B. H., Large-scale pattern growth of graphene films for stretchable transparent electrodes. Nature 2009, 457, 706-10.

69. Yu, H.; Stapleton, A. J.; Lewis, D. A.; Wang, L., High performance flexible metal oxide/silver nanowire based transparent conductive films by a scalable lamination-assisted solution method. Journal of Materiomics 2017, 3, 77-82.

70. Kou, P.; Yang, L.; Chang, C.; He, S., Improved Flexible Transparent Conductive Electrodes based on Silver Nanowire Networks by a Simple Sunlight Illumination Approach. Sci Rep 2017, 7, 42052.

71. Chung, W. H.; Kim, S. H.; Kim, H. S., Welding of silver nanowire networks via flash white light and UV-C irradiation for highly conductive and reliable transparent electrodes. Sci Rep 2016, 6, 32086.

72. Ha, J.; Lee, B. J.; Hwang, D. J.; Kim, D., Femtosecond laser nanowelding of silver nanowires for transparent conductive electrodes. RSC Advances 2016, 6, 86232-86239.

73. Qi. J. S.; Huang. J. Y.; Feng. J.; Shi. D. N.; Li. J.; The possibility of Chemically Inert, Graphene-Based All-Carbon Electronic Devices with 0.8 eV Gap. ACS NANO 2011, 5, 3475-3482

74. Chen, Q.; Zhong, Y.; Zhang, Z.; Zhao, X.; Huang, M.; Zhen, Z.; He, Y.; Zhu, H., Long-term electrical conductivity stability of graphene under uncontrolled ambient conditions. Carbon 2018, 133, 410-415.

75. Deignan, G.; Goldthorpe, I. A., The dependence of silver nanowire stability on network composition and processing parameters. RSC Advances 2017, 7, 35590-35597.

76. Yan, X.; Ma, J.; Xu, H.; Wang, C.; Liu, Y., Fabrication of silver nanowires and metal oxide composite transparent electrodes and their application in UV light-emitting diodes. Journal of Physics D: Applied Physics 2016, 49, 325103.

77. Kim. A.; Won. Y.; Woo. K.; Kim. C. H.; Moon. J., Highly Transparent Low Resistance ZnO/Ag Nanowire/ZnO Composite Electrode for Thin Film Solar Cells. ACS NANO 2013, 7, 1081-1091

78. Ahn, Y.; Jeong, Y.; Lee, Y., Improved thermal oxidation stability of solution-processable silver nanowire transparent electrode by reduced graphene oxide. ACS Appl Mater Interfaces 2012, 4, 6410-4.

79. Liang. J.; Li. L.; Tong. K.; Ren. Z.; Hu. W.; Niu. X.; Chen. Y.; Pei. Q., Silver Nanowire Percolation Network Soldered with Graphene Oxide at Room Temperature and Its Application for Fully Stretchable Polymer Light-Emitting Diodes. ACS NANO 2014, 8, 1590-1600

80. Hu. L.; Kim. H. S.; Lee. J. Y.; Peumans. P.; Cui. Y., Scalable Coating and Properties of Transparent, Flexible, Silver Nanowire Electrodes. ACS NANO 2010, 4, 2955-2963

81. Zhang, Q.; Di, Y.; Huard, C. M.; Guo, L. J.; Wei, J.; Guo, J., Highly stable and stretchable graphene–polymer processed silver nanowires hybrid electrodes for flexible displays. Journal of Materials Chemistry C 2015, 3, 1528-1536.

82. Ahn, Y.; Lee, D.; Jeong, Y.; Lee, H.; Lee, Y., Flexible metal nanowire-parylene C transparent electrodes for next generation optoelectronic devices. Journal of Materials Chemistry C 2017, 5, 2425-2431.

83. Zhao, P.; Kumamoto, A.; Kim, S.; Chen, X.; Hou, B.; Chiashi, S.; Einarsson, E.; Ikuhara, Y.; Maruyama, S., Self-Limiting Chemical Vapor Deposition Growth of Monolayer Graphene from Ethanol. The Journal of Physical Chemistry C 2013, 117, 10755-10763.

84. Galbiati, M.; Stoot, A. C.; Mackenzie, D. M.; Boggild, P.; Camilli, L., Real-time oxide evolution of copper protected by graphene and boron nitride barriers. Sci Rep 2017, 7, 39770.

85. Kim, S. H.; Choi, W. I.; Kim, K. H.; Yang, D. J.; Heo, S.; Yun, D. J., Nanoscale Chemical and Electrical Stabilities of Graphene-covered Silver Nanowire Networks for Transparent Conducting Electrodes. Sci Rep 2016, 6, 33074.

86. Luo, B.; Whelan, P. R.; Shivayogimath, A.; Mackenzie, D. M. A.; Bøggild, P.; Booth, T. J., Copper Oxidation through Nucleation Sites of Chemical Vapor Deposited Graphene. Chemistry of Materials 2016, 28, 3789-3795.

87. Hao. Y.; Bharathi. M. S.; Wang. L.; Liu. Y.; Chen. H.; Nie. S.; Wang. X.; Chou. H.; Tan. C.; Fallahazad. B.; Ramanarayan. H.; Magnuson. C. W.; Tutuc. E.; Yakobson. B. I.; McCarty. K. F.; Zhang. Y. W.; Kim. P.; Hone. J.; Colombo. L.; Ruoff. R. S., The Role of Surface Oxygen in the Growth of Large Single-Crystal Graphene on Copper. Science 2013, 342, 720-723

Academic Achievements

Publications

1. **Yun. H. D.**; Kwak. J.; Kim. S.Y.; Seo. H.; Bang. I. C.; Kim. S. Y.; Kang. S., High performance all-carbon composite transparent electrodes containing uniform carbon nanotube networks., J. Alloy. Compd., 2016, 675, 67-45

2. **Yun. H. D.**; Seo. D. M.; Lee. M. Y.; Kwon. S. Y.; Park. L. S., Effective synthesis and recovery of silver nanowires prepared by tapered continuous flow reactor for flexible and transparent conducting electrode., Metals., 2016, 6, 14

3. Choi. J. K.; Kwak. J.; Park. S. D.; **Yun. H. D.**; Kim. S. Y.; Jung. M.; Kim. S. Y.; Park. K.; Kang. S.; Kim. S. D.; Park. D. Y.; Lee. D. S.; Hong. S. K.; Shin. H. J.; Kwon. S. Y.; Growth of wrinkle-free graphene on texture-controlled platinum films and thermal-assisted transfer of large-scale patterned graphene., ACS NANO., 2015, 9, 679-686

4. Seo. H.; **Yun. H. D.**; Kwon. S. Y.; Bang. I. C., Hybrid graphene and single-walled carbon nanotube films for enhanced phase-change heat transfer., Nano. Lett., 2016, 16, 932-938

5. Park. J.; **Yun. H. D.**; Jin. M. J.; Jo. J.; O. I.; Modepalli. V.; Kwon. S. Y.; Yoo. J. W., Gate-dependent spin hall induced nonlocal resistance and the symmetry of spin-orbit scattering in Au-clustered graphene., Phys. Rev. B., 2017, 95, 245414

6. Nam. H. M.; Seo. D. M.; **Yun. H. D.**; Thangavel. G.; Park. L. S.; Nam. S. Y., Transparent conducting film fabricated by metal mesh method with Ag and Cu@Ag mixture nanoparticle pastes., Metals., 2017, 7, 176

7. 곽진성.; **윤형덕,**; 권순용., 2차원 나노소재의 합성 및 대면적 성장기술., Ceramist 특집., 2017, 20권, 3호, 5-25

8. **Yun et al.,** Unique structure of partially embedded AgNWs in-between multilayer graphene and polyimide for high performance transparent conducting electrodes with long-term stability., to be submitted.

Conference Proceedings and Presentations

1. **Yun.** H. D.; Kwak. J.; Kwon. S. Y., Flexible carbon-based composite electrodes containing uniform carbon nanotube networks., Nano Korea 2015 Symposium., 2015, Seoul, Korea

2. **Yun. H. D.**; Seo. D. M.; Park. L. S.,Synthesis and Laser Patterning of Silver Nanowire for Touch Screen Panel Application., The 15th international meeting on information display., 2015, Daegu, Korea

3. **Yun. H. D.**; Seo. D. M.; Park. L. S., Effective synthesis and recovery of silver nanowires by using continuous flow tapered reactor., The 16th international meeting on information display., 2016, Seoul, Korea

4. **Yun. H. D.**; Seo. D. M.; Park. L. S., Preparation of a high quality polyimide/graphene composite for OLED device fabrication., 2016, Shanghi, China

5. **Yun. H. D.**; Seo. D. M.; Nam. S.; Park. L. S., Effective synthesis of silver nanowires and application to touch screen panel., 2016, Shanghi, China

6. **Yun. H. D.;** Kwak. J.; Kwon. S. Y., Transparent and conducting all-carbon composite electrodes containing uniform carbon nanotube networks for wearable device applications., The 10th international conference on advanced materials and devices., 2017, Jeju island, Korea

7. **Yun. H. D.;** Kwak. J.; Kim. S. Y.; Seo. H.; Bang. I. C.; Kim. S. Y.; Kang. S. T.; Kwon. S. Y., Transparent and conducting all-carbon electrodes with uniform carbon nanotube networks for future wearable device applications., Korea society of LEDs and optoelectronic., 2018, Seoul, Korea

8. **Yun. H. D.;** Kwak. J.; Kim. S. Y.; Seo. H.; Bang. I. C.; Kim. S. Y.; Kang. S. T.; Kwon. S. Y., Transparent and conducting all-carbon electrodes with uniform carbon nanotube networks for future wearable device applications., The Korean ceramic society., 2018, Changwon, Korea

9. Choi. J. K.; Kwak. J. S.; Park. S. D.; **Yun. H. D.**; Kim. S. Y.; Jung. M. B.; Kim. S. Y.; Park. K. B.; Kang. S. T.; Park. D. Y.; Lee. D. S.; Hong. S. K.; Kim. S. D.; Shin. H. J.; Kwon. S. Y., Orientation-sensitive growth of graphene on texture-controlled platinum thin films and thermal-assisted transfer of patterned graphene., The 13th international nanotech symposium., Seoul, Korea

Acknowledgement

First, I would like to thank to my family. My father and mother Sang Ryeol Yun, Hae Hyun Paek, and my younger brother Hyung Suk Yun. With their big support and cheer, I was able to accomplish my Ph.D course in UNIST.

I would like to thank to my advisor, professor Soon-Yong Kwon for giving me an opportunity to study in UNIST as a graduate student. The insights and suggestions with excellent guidance helped me to successfully finish my research thesis.

I would like to thank to professor Lee Soon Park for allowing me to study and experience on various field of research. The expertise and passion professor Lee Soon Park showed me was great chance for me to become as an engineer and scientist.

I also appreciate my thesis committee, professor Heungjoo Shin, professor Kibog Park, Young-Min Kong. Their excellent insights and suggestion helped me to accomplish this thesis.

Finally, huge supports from my graduate colleges in Frontier Innovative Nanomaterials & Devices Laboratory were memorable gifts to me.

Thanks to all graduate students in school of Materials Science and Engineering at Ulsan National Institute of Science and Technology.